Synaptic Mechanisms of Top-Down Control in the Non-Lemniscal Inferior Colliculus

Hannah M. Oberle[1,2], Alexander N. Ford[1], Deepak Dileepkumar[1], Jordyn Czarny[1], & Pierre F. Apostolides[1,3]*
1) Kresge Hearing Research Institute & Department of Otolaryngology, University of Michigan Medical School
2) Neuroscience Graduate Program, University of Michigan
3) Molecular and Integrative Physiology, University of Michigan Medical School
*corresponding author: piaposto@med.umich.edu

Abstract

Corticofugal projections to evolutionarily ancient, sub-cortical structures are ubiquitous across mammalian sensory systems. These "descending" pathways enable the neocortex to control ascending sensory representations in a predictive or feedback manner, but the underlying cellular mechanisms are poorly understood. Here we combine optogenetic approaches with *in vivo* and *in vitro* patch-clamp electrophysiology to study the projection from auditory cortex to the inferior colliculus (IC), a major descending auditory pathway that controls IC neuron feature selectivity, plasticity and auditory perceptual learning. Although individual auditory cortico-collicular synapses were generally weak, IC neurons often integrated inputs from multiple corticofugal axons that generated reliable, tonic depolarizations even during prolonged presynaptic activity. Latency measurements *in vivo* showed that descending signals reach the IC within 30 ms of sound onset, which in IC neurons corresponded to the peak of synaptic depolarizations evoked by short sounds. Activating ascending and descending pathways at latencies expected *in vivo* caused a NMDA receptor dependent, supra-linear EPSP summation, indicating that descending signals can non-linearly amplify IC neurons' moment-to-moment acoustic responses. Our results shed light upon the synaptic bases of descending sensory control, and imply that heterosynaptic cooperativity contributes to the auditory cortico-collicular pathway's role in plasticity and perceptual learning.

Introduction

The auditory system is organized as a network of feedback loops, such that most central auditory nuclei receive descending projections from higher levels of the processing hierarchy (Diamond et al., 1969; Saldaña et al., 1996; Winer et al., 1998, 2001; Doucet et al., 2003; Coomes and Schofield, 2004; Schofield et al., 2006; Suthakar and Ryugo, 2017). The auditory cortex is a major source of excitatory (glutamatergic) descending projections, with the density of descending fibers often rivaling that of ascending fiber tracts (Winer et al., 2001; Winer, 2006; Stebbings et al., 2014). These corticofugal projections likely play a major role in hearing by providing an anatomical substrate for “top-down” information to control early acoustic processing. Indeed, stimulating or silencing the auditory cortex *in vivo* changes spontaneous and sound-evoked activity throughout the central auditory system (Massopust and Ordy, 1962; Ryugo and Weinberger, 1976; Yan and Suga, 1998, 1999; Nwabueze-Ogbo et al., 2002; Xiao and Suga, 2002; Yu et al., 2004; Nakamoto et al., 2008, 2010; Anderson and Malmierca, 2013; Kong et al., 2014; Vila et al., 2019; Blackwell et al., 2020; Qi et al., 2020), indicating that high-level activity regulates the moment-to-moment function of sub-cortical auditory circuits. However, little is known regarding the biophysical properties of auditory corticofugal synapses, nor do we understand how descending signals are integrated with ascending information. Given that synaptic dynamics and pathway integration are fundamental building blocks of neural circuit computations (Abbott et al., 1997; Zucker and Regehr, 2002; Stuart and Spruston, 2015), addressing these knowledge gaps is necessary to understand how the auditory cortex exerts control over early auditory processing.

Of particular interest is the descending projection from auditory cortex to the inferior colliculus (IC), a midbrain hub important for sound localization, speech perception, and an early site of divergence for primary and higher-order auditory pathways (Masterton et al., 1968; Krishna and Semple, 2000; Champoux et al., 2007; Sinex and Li, 2007; Joswig et al., 2015). The IC is generally sub-divided into a “lemniscal” central core and “non-lemniscal” dorsal and lateral shell regions whose neurons have distinct afferent and efferent connections (Faye-Lund and Osen, 1985; Loftus et al., 2008; Ayala et al., 2015; Chen et al., 2018). Whereas central IC neurons project mainly to the primary auditory thalamus (ventral medial geniculate nucleus; Mellott et al., 2014; Oliver, 1984), shell IC neurons preferentially project to secondary, higher-order auditory thalamic nuclei that subsequently funnel acoustic information to the amygdala and striatum (Oliver and Hall, 1978; LeDoux et al., 1990; Bordi and LeDoux, 1994; Mellott et al., 2014; Cai et al., 2019; Ponvert and Jaramillo, 2019). Auditory cortico-collicular axons terminate primarily in the shell IC, with comparatively fewer fibers in the central IC (Bajo et al., 2019; Chen et al., 2018; Lesicko et al., 2016; Song et al., 2018; Winer et al., 1998; Xiong et al., 2015; but see Saldaña et al., 1996). Thus, auditory cortico-collicular synapses seem uniquely positioned to modulate acoustic signals destined for limbic circuits supporting learned valence and habit formation; this prediction is further supported by the fact that chemical ablation of auditory cortico-collicular neurons selectively impairs certain forms of auditory perceptual learning while sparing the performance of previously learned task associations (Bajo et al., 2010). Nevertheless, little is known regarding how auditory cortico-collicular synapses control activity in single IC neurons. Intriguingly, auditory cortex inactivation typically does not abolish IC neuron sound responses, but rather causes divisive, non-monotonic changes in receptive field properties and feature selectivity (Yan and Suga, 1999; Nakamoto et al., 2008, 2010; Anderson and

Malmierca, 2013). Thus, descending transmission might operate in part via heterosynaptic interactions, perhaps by controlling how IC neurons respond to ascending acoustic inputs.

Here we employ electrophysiology and optogenetic approaches to identify how auditory cortico-collicular synapses transmit descending signals, and to understand how descending synapses control IC neuron responses to ascending inputs. We find that the majority of shell IC neurons receive monosynaptic inputs from auditory cortex and often integrate information from multiple distinct corticofugal axons. Synaptic latency measurements *in vivo* show that descending excitation reaches IC neurons ~5-7 ms after spike initiation in auditory cortex, such that cortical feedback will rapidly follow the onset of acoustically driven excitation. Somewhat surprisingly, NMDA receptors only modestly contribute to descending transmission. By contrast, excitatory intra-collicular synapses from the central IC, which are probably a major source of ascending acoustic signals to shell IC neurons, had a much larger NMDA component. Consequently, appropriately timed activity in ascending and descending pathways integrates supra-linearly owing to the cooperative activation of NMDA receptors. Our data reveal a key role for heterosynaptic non-linearities in the descending modulation of early acoustic processing. In addition, the results place important biophysical constraints on the synaptic learning rules that might support the auditory cortico-collicular pathway's role in experience-dependent plasticity and perceptual learning.

Results

Auditory cortico-collicular synapses robustly target superficial IC neurons

Corticofugal axons are predominantly restricted to the shell IC, but little is known about the extent of functional synaptic connectivity between auditory cortex and IC neurons. We tested how auditory cortico-collicular synapses impact IC neurons by transducing the optogenetic activator Chronos in the auditory cortex of mice via intracranial AAV injections (Figure 1A), and 2-4 weeks later, performing *in vivo* whole-cell recordings from the ipsilateral IC of urethane anesthetized mice. GFP-tagged, Chronos expressing auditory cortico-collicular axons were primarily (though not exclusively) restricted to the ipsilateral dorsal-medial and lateral IC (Figure 1-Figure Supplement 1), in agreement with previous studies. Single flashes of blue light from an optic fiber positioned over auditory cortex (1-5 ms duration) reliably triggered excitatory postsynaptic potentials (EPSPs) in n = 21/38 IC neurons recorded from N = 8 mice (Figure 1B). EPSPs were primarily observed in superficial IC neurons, with the majority of unresponsive neurons located more ventrally, presumably in the central IC (Figure 1C; mean depth of cortico recipient and non-recipient neurons: 220 ± 23 vs. 354 ± 38 μm from surface, p=0.0036, Kolmogorov-Smirnov test). A qualitatively similar result was obtained by injecting a trans-synaptic cre virus in auditory cortex of Ai14 tdTomato reporter mice (Zingg et al., 2017, 2020): The majority of anterograde, trans-synaptically labeled IC neurons were located in the dorso-medial and lateral shell regions (N = 3 mice; Figure 1 – Figure Supplement 2), although a few central IC neurons were indeed labeled. Thus, whereas the non-lemniscal shell IC likely receives the most profuse descending inputs from auditory cortex, monosynaptic cortical signals nevertheless likely reach a few neurons in the lemniscal, central IC.

EPSPs in superficial IC neurons had an onset latency of 10.3 ± 0.7 ms following light stimulation (Figure 1D), a peak amplitude of 3.5 ± 0.7 mV (Figure 1E), and a full-width at half-maximum of 18.4

± 1.5 ms (Figure 1F). Interestingly, EPSP amplitudes varied over 2 orders of magnitude across different cells and were occasionally large enough to drive IC neurons beyond spike threshold (Figure 1 – Figure Supplement 3A). These data indicate that bulk activation of corticofugal neurons triggers potent EPSPs in superficial IC neurons. However, under behaviorally relevant conditions, the extent of synaptic depolarization provided by descending inputs will depend on the rate and synchrony of corticofugal neuron firing.

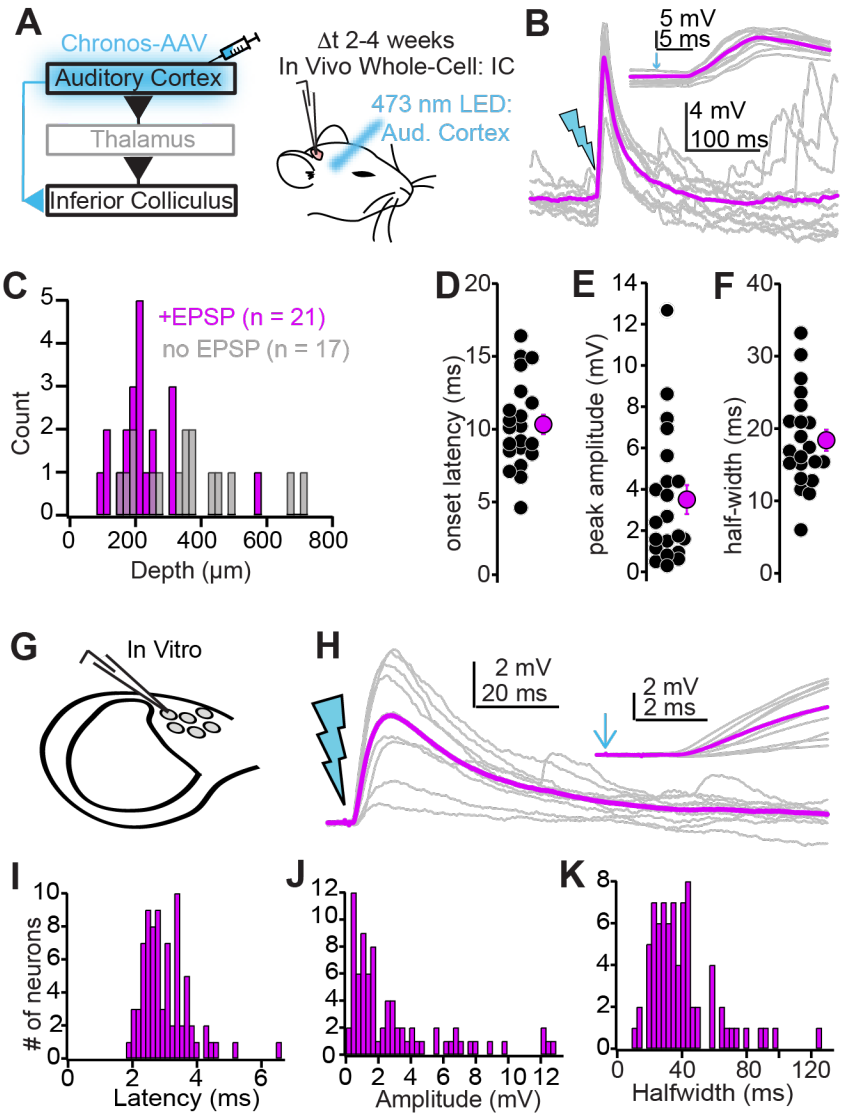

Figure 1: *Biophysical properties of auditory cortico-collicular synapses* **A)** Cartoon of experiment. *In vivo* whole-cell recordings are obtained from IC neurons 2-4 weeks following Chronos injections; an optic fiber is positioned above the auditory cortex. **B)** Example EPSPs following *in vivo* optogenetic stimulation. Gray traces are single trials; magenta is average. Inset is the EPSP rising phase at a faster timebase, arrow denotes light onset. **C)** Dorsal-ventral locations (relative to dura) for IC neurons where auditory cortical stimulation did (magenta) and did not (gray) evoke an EPSP. **D-F)** Summary of EPSP onset (D) amplitude (E), and half-width (F). **G)** whole-cell recordings obtained from dorso-medial shell IC neurons *in vitro*. **H)** EPSPs evoked by *in vitro* optogenetic stimulation (2 ms light flash). Inset: EPSP rising phase. **I-K)** Histograms of EPSP onset (I), amplitudes (J), and half-widths (K) *in vitro*.

Because the auditory cortex projects to many sub-cortical targets besides the IC, *in vivo* stimulation could drive polysynaptic excitation onto IC neurons that would complicate estimates of monosynaptic connectivity. We thus prepared acute IC brain slices from mice injected with Chronos in auditory cortex to quantify the functional properties of descending synapses in a more controlled setting. We targeted whole-cell current-clamp recordings specifically to neurons in the dorso-medial shell IC, as this region shows the highest density of corticofugal axons (Song et al., 2018; our Figure 1 - Figure Supplement 1,2). Stimulating auditory cortico-collicular axons via single blue light flashes delivered through the microscope objective (1-10 ms duration) drove EPSPs in n = 78 neurons from N = 40 mice (Figure 1G,H). EPSPs had short-latency onsets following photo-stimulation (Figure 1I; 3.0 ± 0.1 ms), indicating a monosynaptic rather than polysynaptic origin. EPSPs *in vitro* had a similar range and mean peak amplitude as those recorded *in vivo* (Figure 1J; 2.97 ± 0.35 mV, p=0.3, Mann-Whitney test), and similarly could drive spikes in a subset of recordings (Figure 1 – Figure Supplement 3B). Although the EPSP half-width was significantly slower *in vitro* compared to *in vivo* (Figure 1K; 39.6±2.3 ms, p<0.001, rank-sum test), this result is not surprising: The constant barrage of synaptic inputs *in vivo* is expected to generate a “high conductance state” that accelerates the membrane time constant (Destexhe et al., 2003).

In a separate set of experiments (n = 24 neurons from N = 10 mice), we quantified the kinetics of auditory cortical excitatory postsynaptic currents (EPSCs) as they appear at the soma using voltage-clamp recordings (Figure 1 – Figure Supplement 4. Peak amplitude = 48.1 ± 10.1 pA; weighted decay time constant = 5.8 ± 0.8 ms; 10-90% rise time of 1.3 ± 0.1 ms). Altogether, our results show that auditory cortico-collicular synapses substantially depolarize shell IC neurons independent of network-level, polysynaptic activity. In addition, EPSP kinetics are such that descending excitation will undergo significant temporal summation at firing rates observed during sound-evoked activity of auditory cortico-collicular neurons (20-50 Hz; Williamson and Polley, 2019).

Synaptic strength reflects presynaptic convergence rather than unitary EPSP amplitudes

EPSP amplitudes spanned two orders of magnitude under our conditions (Figure 1E,J). Does this variability reflect a differential potency of individual synapses, or alternatively, differences in the number of presynaptic auditory cortical axons impinging onto individual shell IC neurons? We first estimated unitary EPSP amplitudes using a minimal stimulation paradigm designed to activate one (or very few) auditory cortico-collicular fibers. In these experiments, the LED intensity was titrated to the minimum power required for optogenetic responses to fluctuate between successful EPSPs and failures on a trial-by-trial basis (Figure 2A,B; mean failure rate across experiments: 44 ± 3%, n = 18 cells from N = 14 mice). The mean amplitude of successful EPSPs was generally small (0.84 ± 0.09 mV; Figure 2C) and similar to previous reports of unitary synapses between layer 5 pyramidal neurons in sensory cortex (Brown and Hestrin, 2009; Lefort et al., 2009). By contrast, progressively stronger LED flashes increased the amplitude of successful EPSPs compared to the minimal stimulation condition in many cells tested (n=15 cells from N = 11 mice; Figure 2D,E), indicating that multiple corticofugal axons can converge onto individual shell IC neurons. The ratio of maximum to minimum EPSP showing varied >10-fold across different experiments (median: 1.67, range: 0.91-24.04, Figure 2F), indicating that the EPSP amplitude variability across individual

neurons likely reflects the number of presynaptic auditory cortical fibers recruited during stimulation rather than differences in unitary strength. Importantly, the EPSP half-width was constant across the range of stimulus intensities (Figure 2D, inset. EPSP halfwidth ratios at maximal and threshold LED intensities: 1.04 ±0.07). Similar results were obtained in voltage clamp recordings, with EPSC rise times and half-widths being similar at threshold and maximal LED intensities (Figure 2 – Figure Supplement 1). Together, these results indicate that increased LED intensities recruit more axons rather than prolonging Chronos activation and temporally dispersing vesicle release from single presynaptic boutons. We thus conclude that although the strength of individual auditory cortico-collicular synapses is weak, the convergence of multiple presynaptic fibers ensures that descending signals will substantially increase shell IC neuron excitability.

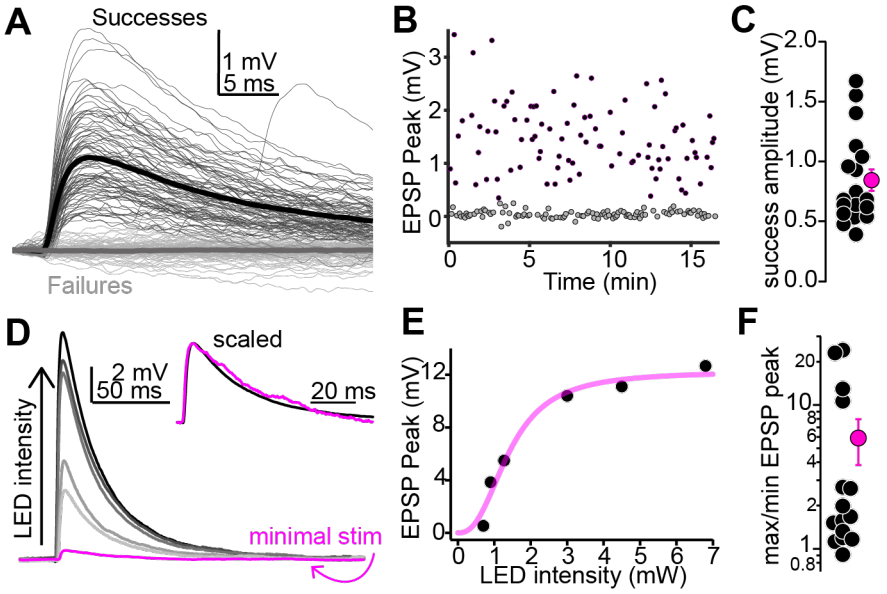

Figure 2: *Multiple auditory cortico-collicular fibers converge onto single shell IC neurons*. **A)** Example threshold optogenetic stimulation experiment. Thin black and gray traces are successes failures, respectively. Thick traces are averages. **B)** Diary plot from the experiment in panel A. black and gray symbols are successes and failures, respectively. **C)** Summary of putative unitary EPSP amplitudes **D)** Magenta: putative unitary EPSP (average of successes recorded at threshold stimulation). Black and Gray traces: averages of successes at increasing LED intensity. Data are from a different neuron as in A. Inset: Peak scaled and onset aligned EPSPs recorded at threshold and maximal intensity, revealing an identical time-course. **E)** EPSP peak amplitude is plotted as a function of LED intensity for the recording in (D). Magenta line is Hill fit. **F)** EPSP amplitude ratios at maximal and threshold LED intensities. Most values are >1, indicating convergence of at least 2 fibers. Of note, data are on a log scale.

Auditory cortico-collicular synapses contact shell IC neurons with diverse biophysical properties

IC neurons have a variety of firing patterns and membrane properties that potentially correspond to distinct neuronal subtypes (Smith, 1992; Peruzzi et al., 2000; Ahuja and Wu, 2007; Moore and Trussell, 2017; Goyer et al., 2019; Naumov et al., 2019; Silveira et al., 2020). However, whether auditory cortico-collicular synapses contact biophysically homogenous or diverse neurons is unknown. We injected 300 ms positive and negative current steps to quantify spiking patterns and passive membrane properties in a subset of our *in vitro* experiments described above (n = 64 cells). 62/64 cortico-recipient shell IC neurons could be classified into one of four general categories. Over half of neurons (38/64) had significant spike rate adaptation during positive current injections

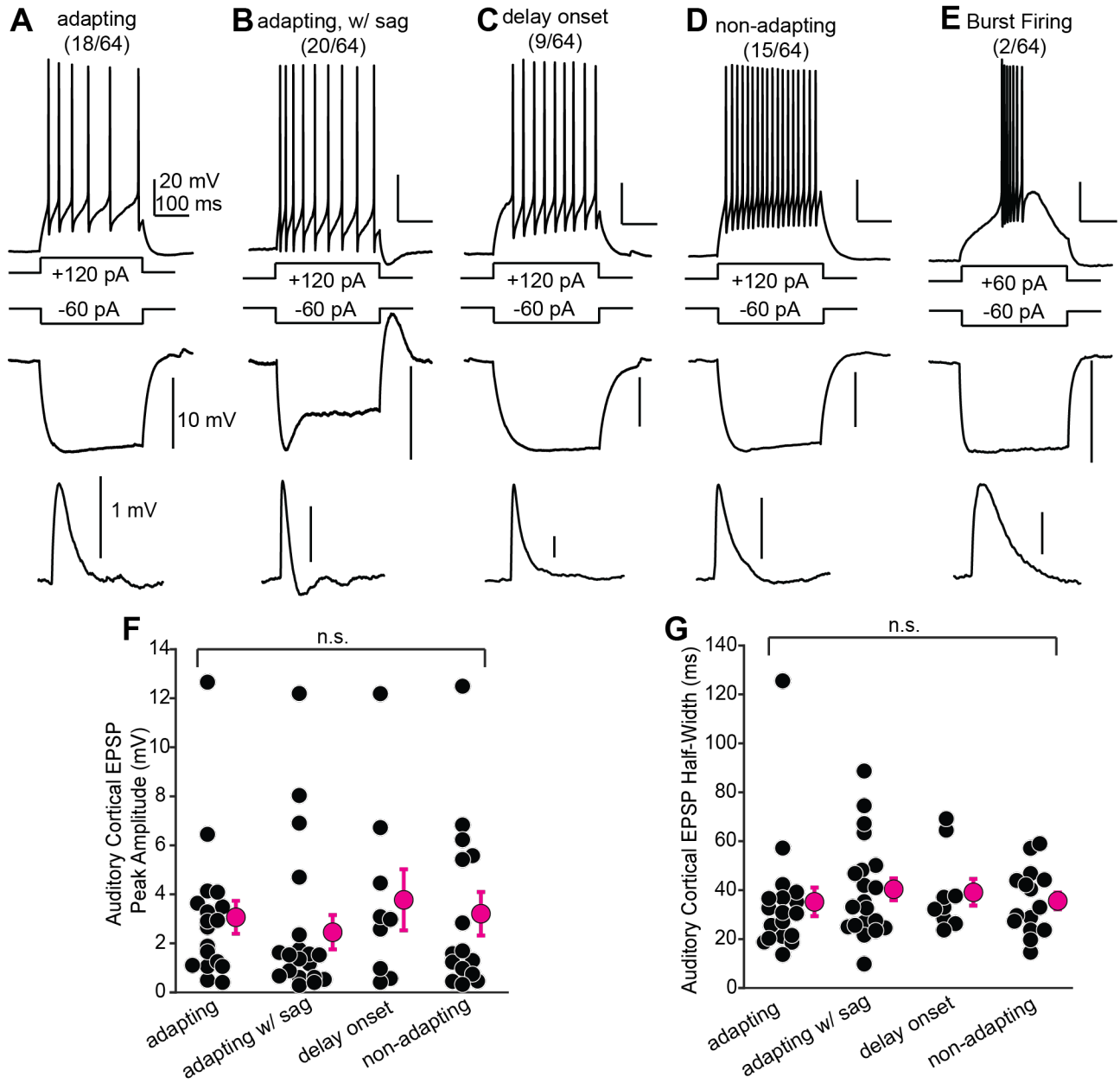

Figure 3: *Shell IC neurons receiving descending signals have diverse biophysical properties.* **A-E)** Examples of different shell IC neurons. Top and Middle traces are spike output and membrane hyperpolarization following positive and negative current steps, respectively. Lower traces: average auditory cortical EPSPs from the same neuron. **F, G)** EPSP peak amplitude (F) and half-width (G) as a function of biophysical category. Bursting neurons are omitted due to low n.

186 (Figure 3A,B) and qualitatively similar firing patterns as the shell IC neurons recorded in rat slices
187 by Smith (1992). However, 18 of these “adapting” neurons responded to negative current with a
188 sustained hyperpolarization (Figure 3A), whereas 20 displayed a prominent I_h-like “sag” likely
189 mediated by HCN channels (Figure 3B, middle trace). These data suggest a minimum of two shell
190 IC neuron sub-types with adapting firing patterns, which can be differentiated based on the extent
191 of I_h sag. By contrast, other neurons had delayed first spikes (9/64, Figure 3C) or showed non-
192 adapting discharge patterns (15/64, Figure 3D). Finally, 2/64 cells displayed a strikingly distinct
193 phenotype, with a burst of spikes riding atop a “hump”-like depolarization similar to neurons
194 expressing T-type Ca^{2+} channels (Figure 3E). EPSP amplitude and half-width of were similar

across the four major categories (Peak amplitude: p=0.45; half-width: p=0.5, Kruskal-Wallis tests) despite marked differences in electrical properties. Thus, the auditory cortex broadcasts similarly strong signals to multiple, putatively distinct IC neurons, arguing that biophysical properties alone do not predict the strength of descending synapses.

Temporal integration of auditory cortical inputs is moderately sub-linear

Auditory cortico-collicular neurons in awake mice respond to acoustic stimuli with ~10-50 Hz spike trains (Williamson and Polley, 2019). Given the kinetics of auditory cortico-collicular EPSPs (Figure 1), these spike rates are expected to result in significant temporal summation of descending signals. However, the use-dependent dynamics neurotransmitter release, as well as postsynaptic ion channels, can enforce sub- or supra-linear summation that effectively dictates the temporal integration of EPSPs (Markram et al., 1998; Polsky et al., 2009). How do IC neurons integrate sustained cortical activity? We addressed this question by repetitively stimulating auditory cortico-collicular axons (10 light pulses at 20 or 50 Hz, 2 ms pulse width; Figure 4A,B, black traces; n = 12 neurons from N = 7 mice). We quantified temporal integration by comparing the peak EPSP amplitudes observed after each light flash in the train to the amplitudes expected from the linear summation of a single auditory cortico-collicular EPSP recorded in the same neuron (Figure 4A,B; magenta traces). The observed peak amplitude of the 10th EPSP in the train reached 92 ± 13 % and 77 ± 16% of that expected from linear summation at 20 and 50 Hz, respectively (Figure 4C,D). These results argue that at the population-level, auditory cortical firing rates are read out as moderately sub-linear shifts of the membrane potential towards threshold. These sub-linear effects were likely due to frequency-dependent synaptic depression, as the trough-to-peak amplitude of individual EPSPs during train stimulation showed greater reduction at faster rates (Figure 4 – Figure Supplement 1; EPSP 10/EPSP 1: 83 ± 10 % vs. 39 ± 9% for 20 and 50 Hz trains, respectively. p<0.001, sign-rank test).

Auditory cortico-collicular neurons display elevated firing rates at ~20 Hz for the entirety of long-duration, complex sounds (e.g., 4 s long dynamic chord stimuli; Williamson and Polley, 2019). We thus wondered if descending synapses maintain transmission during sustained acoustic processing, or if synaptic depression instead limits descending signals to sound onset. Stimulating auditory cortical axons with 4 s trains of light pulses at 20 Hz (Figure 4E) drove fast EPSPs riding atop a steady-state, tonic depolarization (Figure 4F; mean amplitude of DC component during the final 1 s of stimulation: 1.18 ± 0.01 mV, p = 0.013, one-sample t-test compared to a hypothetical value of 0. n = 10 cells from n = 7 mice). Importantly, these effects were not an artifact of directly stimulating auditory cortico-collicular nerve terminals in brain slices: A similar tonic depolarization was observed in superficial IC neurons recorded *in vivo* using an optic fiber positioned over auditory cortex (Figure 4G,H; mean amplitude of DC component: 1.5 ± 0.7 mV, n=19 cells from n = 6 mice, p=0.53 compared to *in vitro* data, rank-sum test).

In addition, cessation of cortical stimulation *in vivo* also caused a long-lasting after-hyperpolarization (AHP) in 14/19 cells: The membrane potential rapidly fell below baseline after the last stimulus (τ = 76.5 ± 1.5 ms) and recovered over several seconds (τ = 2.6 ± 0.6 s; Figure 4 – Figure Supplement 2). Interestingly, this AHP was independent of postsynaptic spiking and thus may reflect buildup of feed-forward inhibition from local and long-range sources, or alternatively, a

transient cessation of tonic descending excitation. Altogether, these experiments show that auditory cortico-collicular synapses can sustain transmission on seconds time scales via tonic and phasic excitation. In addition, the profound AHP following *in vivo* stimulation suggests that IC neuron

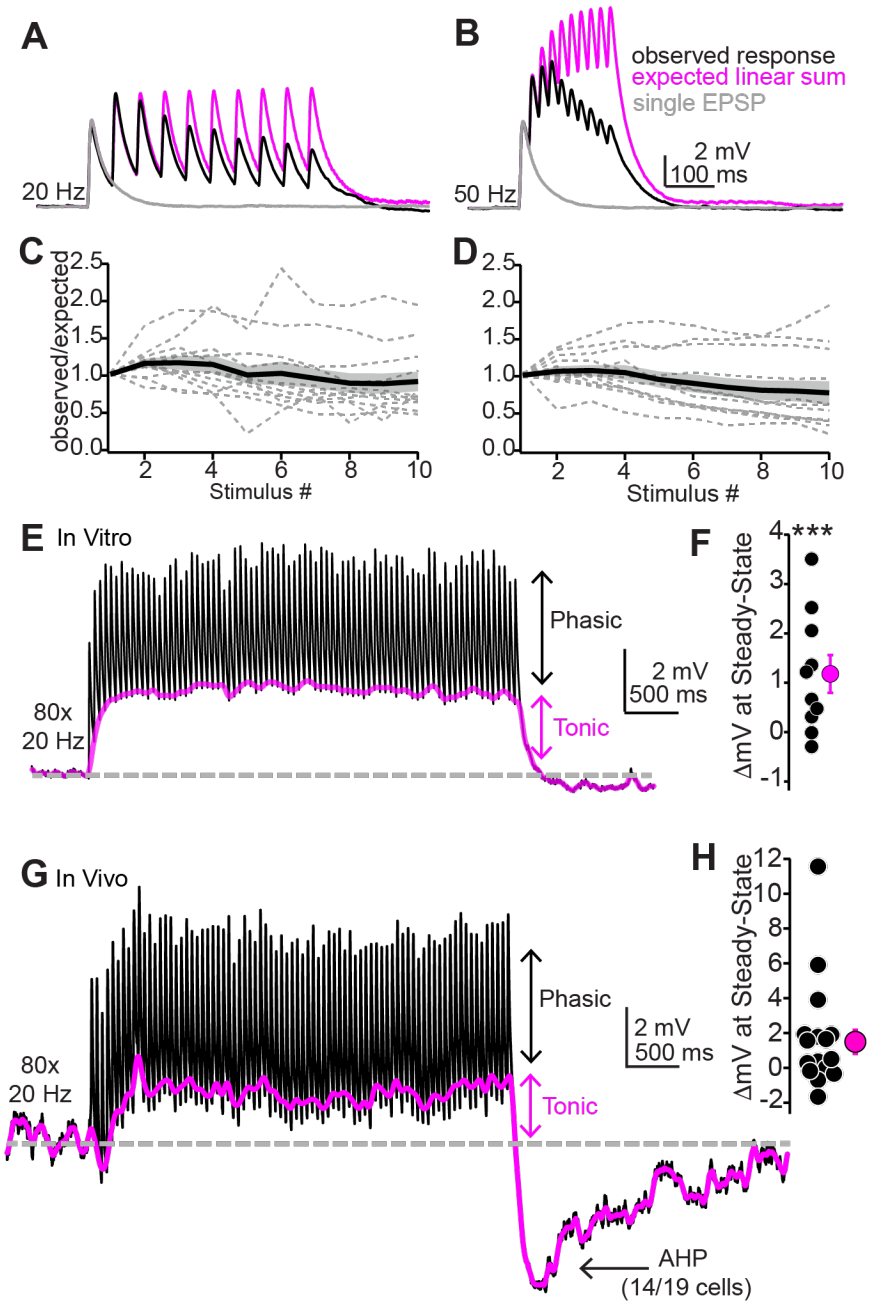

Figure 4: *Repetitive synaptic activity tonically depolarizes shell IC neurons despite sub-linear temporal summation of EPSPs.* **A,B)** Black traces: Average EPSPs evoked by 20 (A) or 50 Hz (B) trains of 10 light flashes. Gray: Average EPSPs evoked by a single 2 ms light flash recorded in the same neuron. Magenta: The expected response assuming linear summation of single EPSPs at each frequency. Of note is that the recorded EPSP amplitudes in the train are smaller than the expected linear sum. Data in A and B are from the same neuron. **C,D)** Summary of observed over expected amplitudes for EPSPs during 20 (C) or 50 Hz (D) trains. Gray dotted lines are individual neurons; black + shading are mean ± SEM **E)** Sustained auditory cortical transmission generates phasic EPSPs (black) riding atop a tonic depolarization (magenta) *in vitro*. **F)** Group data quantifying membrane potential changes at steady-state (final 1 s of stimulation). **G,H)** Same as E and F but during *in vivo* recordings. Of note is the large AHP.

excitability is bi-directionally yoked to auditory cortical firing patterns. Thus, increases as well as pauses in auditory cortico-collicular neuron activity may be comparably significant to IC neurons.

NMDA receptors contribute to temporal integration of descending signals

Central excitatory transmission is predominantly mediated by AMPA and NMDA type glutamate receptors, with NMDA receptors being particularly crucial for dendritic integration, associative plasticity, and learning. The auditory cortico-collicular pathway is involved in perceptual learning following monaural hearing loss (Bajo et al., 2010), and NMDA receptors in the avian IC shell homologue preferentially contribute to receptive fields generated by experience-dependent plasticity (Feldman et al., 1996). We thus asked to what extent auditory cortico-collicular synapses activate NMDA receptors in shell IC neurons. Interestingly, bath application of the AMPA/kainate receptor antagonist NBQX (10 μM) completely abolished EPSPs in all neurons tested (Figure 5A,B. Peak amplitude control: 1.93 ± 0.02 mV; NBQX: 0.09 ± 0.03 mV, p=0.004, n=9 cells from N = 7 mice, Wilcoxon sign-rank test), indicating that AMPA receptors mediate the overwhelming majority of synaptic depolarization at descending synapses.

By contrast, although the NMDA receptor antagonist R-CPP (5 μM) had minimal effect on the peak amplitude of auditory cortico-collicular EPSPs evoked with single light flashes (Figure 5C,D; n = 9 cells from N = 6 mice. Control: 3.3 ± 0.9 mV, R-CPP: 3.4 ± 0.9 mV, p = 0.67, paired t-test), R-CPP caused a modest but significant reduction in the EPSP half-width (Figure 5C,E; control: 35.7 ± 4.4 ms, R-CPP: 30.4 ± 4.7 ms. 17.6% reduction, p=0.016, paired t-test). This modest effect of R-CPP in current clamp recordings was not due to a complete absence of NMDA receptors at descending synapses, nor was it due to the presence of R-CPP resistant NMDA receptors (Feng et al., 2005): Depolarizing neurons to +30 to +45 mV in voltage-clamp (using a Cs^+-rich internal solution) slowed the weighted decay time constant of optogenetically evoked EPSCs by 8.2 fold compared to negative holding potentials (Figure 5 – Figure Supplement 1A,B; -60 to -70 mV: 6.1 ± 0.9 ms, +30 to +40 mV: 50.0 ±0.8 ms, n = 5 cells from N = 3 mice), consistent with the biophysical properties of NMDA receptors. Furthermore, R-CPP markedly accelerated the decay tau of EPSCs recorded at positive potentials (Figure 5 – Figure Supplement 1C,D; n = 7 cells from N = 4 mice. Control: 70.1 ± 17.6 ms, R-CPP: 10.2 ± 1.3 ms, p= 0.0156, sign-rank test). The remaining fast EPSC was abolished by NBQX (n = 3 cells from N = 2 mice), indicating that at the concentration applied (5 μM), R-CPP fully saturates NMDA receptors at auditory cortico-collicular synapses. We conclude that although AMPA receptors mediate the bulk of descending transmission at resting membrane potentials, glutamate released from descending synapses nevertheless reaches synaptic NMDA receptors to shape EPSP kinetics. Thus, although NMDA receptors contribute little to the peak amplitude of EPSPs during sparse stimulation, they may nevertheless control the integration of repetitive activity across time.

Accordingly, R-CPP significantly reduced summation of auditory cortico-collicular EPSPs evoked by a train of 10 stimuli at 50 Hz (Figure 5F, G; n=10 cells from N = 8 mice. Main effect of drug condition in a two-way repeated measures ANOVA; F(1,9)=5.91, p=0.038), resulting in a 26% reduction in the cumulative integral of the synaptic depolarization (Figure 5F,H; control: 1.42 ± 0.35 mV * s, R-CPP: 1.03 ± 0.26 mV * s; p=0.012, paired t-test). These data show that NMDA receptors

prolong the integration time window for descending signals, thereby boosting postsynaptic depolarizations during sustained cortical activity.

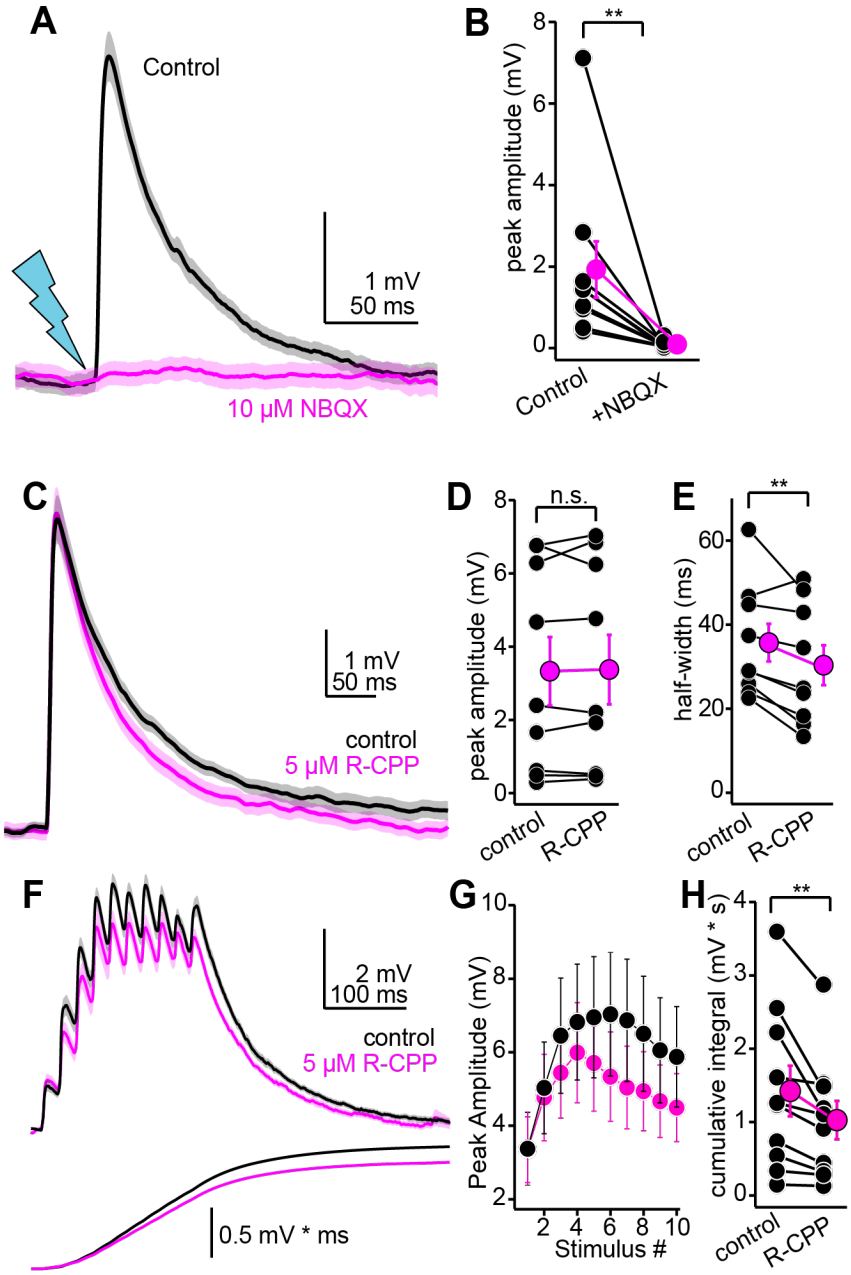

Figure 5. *Pharmacology of descending transmission.* **A)** EPSPs (mean ± SEM) from a single neuron before (black) and after (magenta) bath application of NBQX (10 μM). Of note is the absence of residual synaptic depolarization after NBQX. **B)** Summary data. For the effect of NBQX on descending EPSPs. **C)** EPSPs before and after R-CPP (black and magenta traces, respectively). **D, E)** Group data for the effect of R-CPP on EPSP peak amplitude (D) and half-width (E). Asterisks denote statistical significance. **F)** Upper panel: EPSPs (average ± SEM) evoked by 10 light flashes at 50 Hz. Black and magenta are in control and R-CPP. Lower panel is the cumulative integral of the waveforms. **G)** Group data showing amplitude of each EPSP in the train (mean ± SEM) before and after R-CPP (black and magenta, respectively). **H)** Group data for the effect of R-CPP on voltage integral as in F. Asterisks denote significance.

Differential contribution of NMDA receptors at ascending and descending synapses

The modest contribution of NMDA receptors at descending synapses is surprising, as previous studies suggest a rather prominent NMDA component at excitatory synapses in the IC (Smith, 1992; Wu, 2004). We thus wondered if our results reflected a relative paucity of NMDA receptors at all excitatory synapses onto shell IC neurons, or rather a unique feature of auditory cortico-collicular synapses. Shell IC neurons receive a prominent intra-collicular projection from the central IC which likely transmits a significant amount of ascending acoustic information (Saldaña et al., 1996; Sun and Wu, 2009). We tested if the NMDA component differed between ascending and descending EPSPs in the same neuron using a dual pathway stimulation approach *in vitro*: A bipolar stimulating electrode was positioned in the central IC and Chronos was expressed in auditory cortex to activate ascending and descending synapses, respectively (Figure 6A). 2.5-5 µM gabazine was present in all experiments to isolate excitatory transmission. Repetitive stimulation of either pathway (5x, 50 Hz) led to summating EPSPs which were differentially sensitive to NMDA receptor blockade (Figure 6B-C): 5 µM R-CPP reduced the cumulative integral of central IC and auditory cortical EPSPs to 44±4% and 78±4% of baseline, respectively (Figure 6D, n=9 cells from n = 8 mice, p=0.0004, paired t-test), indicating that NMDA receptors contributed less at descending compared to ascending synapses. These results were not solely due to greater contribution of NMDARs during train stimuli at ascending compared to descending synapses. Indeed, qualitatively similar results were also observed in a between cell comparison of R-CPP effects on ascending and descending EPSPs evoked with single stimuli: R-CPP caused a significantly greater reduction in the peak amplitude of ascending EPSPs evoked with single shocks compared to the auditory cortical EPSPs evoked with single light flashes in experiments of Figures 5C-E (Figure 6-Figure Supplement 1A,B. Fraction peak amplitude remaining in R-CPP: 75 ± 5 vs. 103 ± 4%, n = 8 cells from N = 5 mice vs. n = 9 cells from N = 6 mice for central IC and auditory cortical inputs, respectively. p<0.001, unpaired t-test). Similarly, the half-width of single ascending EPSPs was modestly, albeit significantly more reduced by R-CPP compared to single descending EPSPs (Figure 6 – Figure Supplement 1C. Fraction halfwidth remaining in R-CPP: 64 ± 5 vs. 82 ± 5% for central IC and auditory cortical inputs, respectively. p = 0.024, paired t-test). Thus, the extent of NMDA receptor contribution to

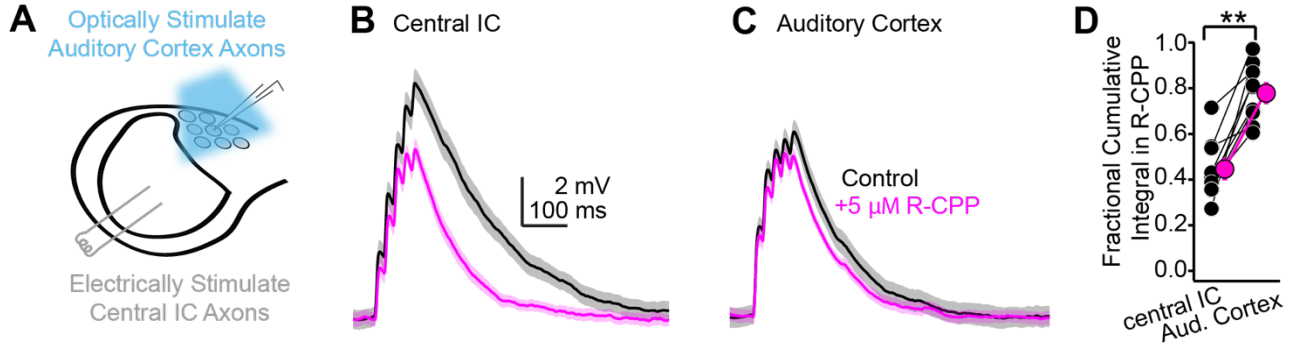

Figure 6. *Differential contribution of NMDA receptors at ascending and descending synapses.* **A)** Cartoon of experiment: Blue light flashes delivered through the microscope objective activate descending auditory cortico-collicular axons; a bipolar electrode in the central IC stimulates ascending central ->shell IC axons. **B,C)** EPSPs evoked by 5x 50 Hz stimulation of central IC (B) or auditory cortex (C) axons, in absence or presence of R-CPP (black and magenta, respectively). Data in panels B and C are from the same neuron. **D)** Group data quantifying the fractional EPSP remaining in R-CPP (as measured by the cumulative integral of the EPSP waveform) for central IC and auditory cortico-collicular synapses.

descending transmission reflects a synapse-specific property of auditory cortico-collicular inputs rather than the global distribution of NMDARs in shell IC neurons.

Auditory cortical inputs are predicted to arrive at the peak of EPSPs evoked by transient sounds

Layer 5 auditory cortico-collicular neurons in awake mice respond to sound with a mean first-spike latency of ~21 ms (Williamson and Polley, 2019). This value is surprisingly shorter than reported first spike latencies in shell IC neurons (~35 ms; Lumani and Zhang, 2010). Whether auditory cortical excitation arrives before, during, or after the onset of sound-evoked EPSPs in shell IC neurons effectively determines how ascending and descending signals integrate at the single cell level, but the relative timing of distinct inputs onto IC neurons is unknown. We thus quantified the relative timing of ascending sound-evoked and descending cortical EPSPs using *in vivo* whole-cell recordings from superficial IC neurons of anesthetized mice. We first determined the onset latency of descending EPSPs in IC neurons using electrical stimulation of the auditory cortex (Figure 7A). We employed electrical, rather than optogenetic stimulation for these experiments because spike onset following optogenetic stimulation is limited by the cell's membrane time constant and effective spike threshold, whereas electrical stimulation bypasses somato-dendritic depolarization by directly triggering axonal spikes. Single shocks delivered to the auditory cortex evoked EPSPs with an onset latency of 5.4 ± 0.6 ms (n = 7 cells from n = 4 mice; mean depth of recorded neurons 188 ±

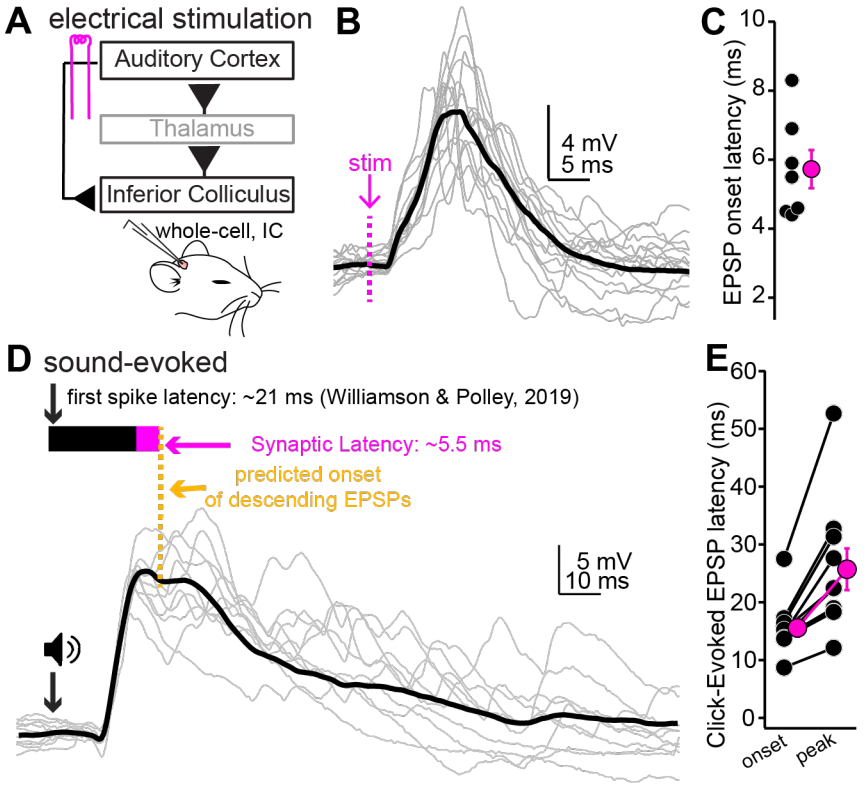

Figure 7: *Auditory Cortical feedback is predicted to collide with the peak of ascending excitation.* **A**) Cartoon of experiment. **B)** Example recording showing short latency EPSPs following a single shock to the auditory cortex. Dotted line is onset of stimulation. Gray traces are single trials; black is average. The stimulation artifact, as well as APs riding atop the cortical EPSP, were blanked for clarity. **C)** Group data for EPSP onset latency. **D)** EPSPs evoked by a 200 µs click. Arrow and speaker show sound onset. Data are from a different neuron than in B. Black and magenta bars above the traces show the reported first spike latency of auditory cortico-collicular neurons from previous work and the synaptic latency calculated from panels B and C, respectively. **E)** Group data for onset and peak latency of click-evoked EPSPs.

14 μm, Figure 7B,C), indicating that descending information reaches IC neurons within a few ms of AP initiation in auditory cortex. Since the mean first-spike latency of auditory cortico-collicular neurons is ~21 ms (Williamson & Polley, 2019) and the synaptic latency is 5-8 ms (Figure 7B,C), these data collectively argue that that cortical feedback begins to excite IC neurons <30 ms after sound onset. Furthermore, assuming an axon path length of ~8 mm from auditory cortex to shell IC (Llano et al., 2014) and a synaptic release delay of ~2 ms, the data suggest a minimum conduction velocity of ~2.35 m/s under these conditions. These values are similar to conduction velocity estimates for the myelinated axons of layer 5 pyramidal neurons in rodents (2.9 m/s; Kole et al., 2007), suggesting that layer 5, and not unmyelinated layer 6 neurons, are the dominant source of descending signals to the IC.

We next calculated the timing of sound-evoked excitation onto superficial IC neurons using broadband “click” transients (Figure 7D, n = 10 cells from N = 7 mice. Mean depth: 204±23 μm). Although sound-evoked EPSPs were typically sub-threshold under our conditions, click stimuli occasionally drove spikes in 5/10 experiments (33.8 ± 16.6% of trials), with mean first spike latencies of 29.4±7.6 ms. These values are similar to previous studies in anesthetized animals showing that sound-evoked spiking of shell IC neurons is sparse (Lumani and Zhang, 2010; Geis et al., 2011; Valdés-Baizabal et al., 2021). Sound evoked EPSPs had mean onset and peak latencies of 15.5 ± 1.5 and 25.7 ± 3.6 ms, respectively (Figure 7E), indicating that cortical feedback lags the rising phase of sound-evoked excitation by a mere 10-15 ms. These conclusions are unlikely to reflect idiosyncratic artifacts of anesthesia, as the onset of click-evoked local field potentials (LFPs) were similar in awake and anesthetized mice (Figure 7 – Figure Supplement 1. 9.70 ± 0.36 vs. 9.16 ± 0.32 ms in N = 11 awake and N = 8 anesthetized mice, respectively, p = 0.31, unpaired t-test). Furthermore, although brain state can affect conduction velocity of cortical axons (Stoelzel et al., 2017), spike propagation is generally *faster* during high compared to low arousal levels. Our latency estimates (Figure 7B,C) thus likely represent an upper bound for the arrival of descending cortical signals in awake states.

The data of Figure 7 suggest that cortical excitation arrives in IC neurons prior to, or in very close succession with, the peak of EPSPs evoked by transient sounds. Moreover, the 5-10 Hz spontaneous firing rate of layer 5 pyramidal neurons *in vivo* (O’Connor et al., 2010; Yavorska and Wehr, 2021) suggest that auditory cortex activity prior to sound onset could modulate the earliest phases of acoustic activity in the IC. We thus tested if auditory cortex inactivation via cooling impacts sound-evoked activity in the superficial IC of awake mice (Figure 7 – Figure Supplement 2A,B). Accordingly, bilateral cooling of the auditory cortices using peltier devices reversibly reduced the slope of click-evoked LFPs (Figure 7 – Figure Supplement 2C,E; n = 11 recordings in N = 6 mice. One-way repeated measures ANOVA, $F(1.402,14.02)=13.89$, $p=0.0011$). In addition, 9 out of these 11 recordings also had measurable multi-unit spike activity whose rates increased following click sounds (Figure 7 – Figure Supplement 2B,D). Consistent with the LFP data, the onset of click-evoked multi-unit activity was reversibly delayed by auditory cortical cooling (Figure 7 – Figure Supplement 2D,F; n=9 recordings in N = 6 mice. One-way repeated measures ANOVA, $F(1.294,10.35)=26.15$, $p=0.0002$). Altogether, these results indicate that auditory cortical activity substantially impacts how IC neurons respond to transient sounds.

NMDA receptor dependent, supra-linear pathway integration in shell IC neurons

Our latency measurements (Figure 7) suggest that ascending information is rapidly followed by descending cortical excitation. This temporal overlap is intriguing because ascending and descending synapses express NMDA receptors (Figure 6), which in other cell-types, enable cooperative interactions between co-active pathways onto the same neuron (Takahashi and Magee, 2009). We thus hypothesized that appropriately timed cortical feedback might integrate non-linearly with ascending inputs from the central IC, thereby generating a synaptic depolarization larger than expected from the sum of either pathway active in isolation. We tested this idea *in vitro* using our dual pathway stimulation approach (Figure 6) while recording from shell IC neurons. We first recorded the synaptic depolarization following stimulation of ascending and descending pathways in isolation (5 stimuli at 50 Hz; Figure 8A, upper traces). We next simultaneously activated the two pathways such that the onset of cortical EPSPs collided with the peak of ascending EPSPs, as predicted from our *in vivo* latency measurements (Figure 7). The observed depolarization during synchronous pathway activation was on average significantly larger than expected from the arithmetic sum of each pathway stimulated alone (Figure 8A; n=12 cells from N=9 mice. Cumulative integral observed: 1.90 ± 0.35 mV*ms, expected: 1.45±0.22 mV*ms, p=0.007, paired t-test test), indicating that coincident activity of ascending and descending pathways summates supra-linearly. Importantly, R-CPP mostly abolished this supra-linear summation, such that the depolarization during coincident activation in R-CPP now equaled the expected sum of each pathway activated alone (Figure 8B,C, lower traces; n=7 cells from N = 7 mice. Observed/Expected control: 1.39±0.05; in R-CPP: 1.02±0.04, p=0.0156, sign-rank test). Thus, synaptic NMDA receptors provide a supra-linear boost when descending excitation follows

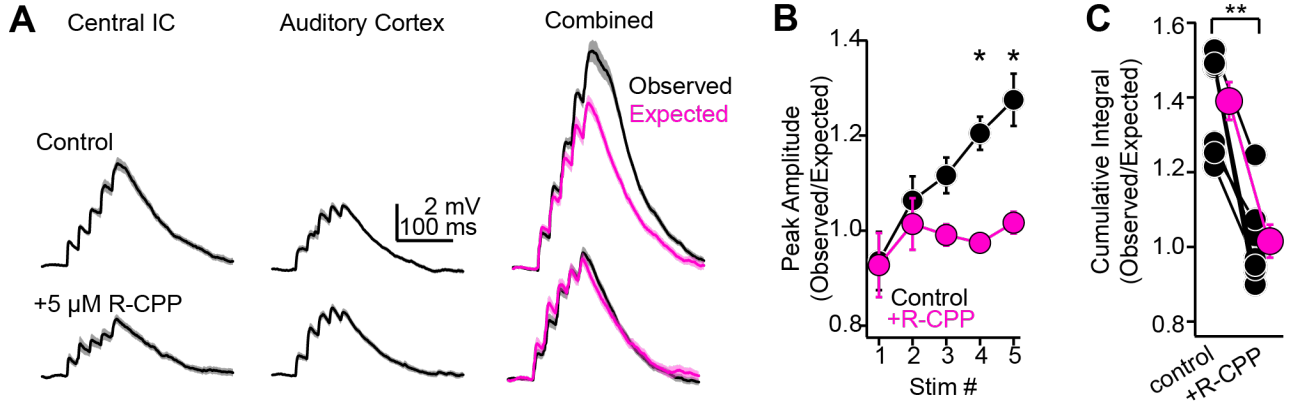

Figure 8: *NMDA-receptor dependent, supralinear pathway integration.* **A)** Upper and lower traces are during baseline conditions and after bath applying R-CPP. Left and middle panels: EPSPs during electrical or optogenetic stimulation of central IC or auditory cortical axons, respectively (5x, 50 Hz stimuli). Right panel ("Combined"): Black traces are the observed depolarization during simultaneous stimulation of both pathways. Magenta is the depolarization expected from the arithmetic sum of the waveforms following stimulation of either pathway alone (e.g., left and middle traces). Of note, the observed depolarization under control conditions is larger than expected from linear summation; blocking NMDA receptors linearizes pathway integration (compare black and magenta traces in R-CPP). **B)** Group data plotting the ratio of observed and expected peak amplitude for each of 5 EPSPs in a 50 Hz train during synchronous activation of central IC and auditory cortical synapses. Asterisks denote statistical significance of Bonferroni post-hoc test for the fourth and fifth stimuli following a main effect of drug condition (p=0.038, F(1,9), Two-way repeated measures ANOVA). **C)** Group data, observed over expected ratio of the cumulative integral during combined pathway activation in control conditions and in the presence of R-CPP. Asterisks denote statistical significance (sign-rank test).

ascending activity, thereby promoting the non-linear mixing of distinct pathways in single IC neurons.

Discussion

We have shown that the majority of neurons in the superficial (shell) IC layers receive reasonably strong excitation from auditory cortex that is predicted to arrive within 30 ms following sound onset. Given the relatively long latency of sound-evoked PSPs in shell IC neurons (our Figure 7D,E; see also Valdés-Baizabal et al., 2021), we suggest that descending signals arrive near the peak of ascending excitation evoked by short sounds. However, our measurements of corticofugal latencies likely represent an upper bound for descending transmission, as our experiments were performed under anesthesia; the conduction velocity of cortical axons is generally increased in alert compared to non-alert animals (Stoelzel et al., 2017), such that corticofugal excitation may arrive at the IC substantially faster in awake, behaving animals.

Cooling the auditory cortex slowed the rising slope of sound-evoked LFPs in awake mice, as originally observed by Nwabueze-Ogbo et al., 2002 using pharmacological inactivation in anesthetized rats. In addition, cortical cooling substantially delayed the onset of sound evoked spiking in the IC. A potential explanation is that in addition to rapid feedback following sound onset, the behaviorally modulated, ~5-10 Hz spontaneous firing of layer 5 corticofugal neurons (O'Connor et al., 2010; Yavorska and Wehr, 2021) may predictively dictate how IC neurons respond to incoming brainstem signals. Indeed, descending transmission is maintained during extended activity periods (Figure 4), which may allow the cortex to tonically depolarize IC neurons as a function cortical state. However, an important caveat is that our cooling approach also likely impacted corticofugal transmission to the cochlear nuclei and superior olive. Although sub-tectal corticofugal projections are comparatively sparser than the auditory cortico-collicular pathway (Weedman and Ryugo, 1996; Doucet et al., 2003; Coomes and Schofield, 2004), a formal possibility nevertheless remains that some of our observed effects are due to modulation of ascending brainstem inputs to the IC.

Our data suggest that shell IC neurons are the major target of auditory cortico-collicular fibers. However, the non-uniform thickness of the IC shell across medial-lateral axis (Barnstedt et al., 2015) indicates we cannot rule out that some of our *in vivo* data are from neurons in the most dorsal region of the central IC. Indeed, *in vivo* intracellular recordings from neurons in the deep IC layers report EPSPs following auditory cortex stimulation (Mitani et al., 1983; Qi et al., 2020), implying that some functional cortical synapses may in fact target central IC neurons. However, *in vitro* circuit mapping experiments imply that monosynaptic connections between auditory cortex and central IC may be rare (Xiong et al., 2015; Song et al., 2018), and our trans-synaptic labeling and *in vivo* electrophysiology data support the conclusion that shell IC neurons process the bulk of descending signals. However more thorough functional circuit-mapping studies are needed to directly quantify the extent and synaptic potency of descending inputs in specific IC sub-divisions.

Interestingly, a recent study suggested that vasoactive intestinal peptide (VIP) expressing GABAergic interneurons in auditory cortex send axonal projections to the shell IC (Bertero et al.,

2021). In our conditions, the AMPA/kainate receptor antagonist NBQX largely abolished descending transmission (Figure 5); we did not observe any inhibitory postsynaptic potentials in the presence of NBQX, as would be expected from the direct stimulation of GABAergic axons. However, these newly identified corticofugal GABAergic synapses have low release probability, signal mainly via “spillover” transmission (Isaacson et al., 1993; Szabadics et al., 2007), or operate via the release of VIP which would be difficult to quantify with our methods. Future studies are required to disentangle the relative contributions of glutamatergic and GABAergic corticofugal transmission in the IC.

Synapse-specific contribution of NMDA receptors in shell IC neurons

The minor contribution of NMDA receptors to auditory cortico-collicular transmission is somewhat surprising, as synaptic NMDA receptors are activated even at hyperpolarized membrane potentials in central IC neurons (Ma et al., 2002; Wu, 2004; Goyer et al., 2019; Kitagawa and Sakaba, 2019). However, our results do not simply reflect a global paucity of NMDA receptors at excitatory synapses onto dorso-medial shell IC neurons, but rather can be explained by a pathway specific contribution of specific glutamate receptor sub-types to the synaptic depolarization: NMDA receptor blockade reduced EPSPs to a greater extent at central IC -> shell IC compared to auditory cortico-collicular synapses. Although a simple explanation is that the total number of synaptic NMDA receptors in shell IC neurons differs in a pathway specific manner, we cannot exclude differences in NMDA receptor subunit composition (Schwartz et al., 2012), glutamate diffusion (Arnth-Jensen et al., 2002), and synapse location (Branco et al., 2010; Song et al., 2018) as contributing factors.

Non-linear integration of ascending and descending signals

Intra-collicular synapses originating from the central IC likely provide a significant amount of ascending acoustic input to shell IC neurons. Indeed, reported first spikes latencies of central IC neurons typically lead the onset of sound evoked EPSPs in shell IC neurons (Syka et al., 2000; Hurley and Pollak, 2005), and central IC neurons send tonotopically organized axonal projections to the IC shell that conspicuously mirror the tonotopic distribution of best frequencies in the shell IC (Saldaña and Merchán, 1992; Wong and Borst, 2019). By contrast, the onset of sound-evoked EPSPs in shell IC neurons typically begin prior to the reported first spikes of auditory cortico-collicular neurons, thereby ruling out the possibility that acoustic responses are solely inherited from auditory cortex. Instead, axonal conduction velocities along ascending and descending pathways impose an obligatory delay such that cortical feedback excitation arrives ~25-30 ms following the onset of sound-evoked EPSPs. Notably, while glutamate released from ascending terminals will have unbound and diffused away from low-affinity synaptic AMPA receptors prior to the onset of cortical feedback excitation (Clements et al., 1992), high-affinity NMDA receptors are expected to remain bound with glutamate during this time (Lester and Jahr, 1992). Extracellular Mg^{2+} imparts a voltage-dependence to the NMDA receptor channel; the additional depolarization provided by cortical feedback would thus be expected to cooperatively enhance current flowing through NMDA receptors at ascending synapses active immediately prior to the onset of cortical feedback. This prediction is supported by our data showing a NMDA receptor-dependent, supra-linear summation of ascending and descending inputs that are activated similar to their expected timing *in vivo*. These single-cell, biophysical operations can potentially explain the non-linear changes in IC neuron receptive fields during cortical inactivation (Yan and Suga, 1999; Nakamoto

et al., 2008, 2010). An important avenue for future research will be to determine how other voltage-gated channels contribute to integrative non-linearities in IC neurons. Indeed, although the NMDA receptor antagonist R-CPP largely abolished our observed effects, we did not formally investigate the role of other dendritic conductances such as Na^+ (Stuart and Sakmann, 1995; Apostolides and Trussell, 2014; Hsu et al., 2018) or Ca^{2+} channels (Takahashi and Magee, 2009; Fletcher and Williams, 2019) in synaptic integration.

NMDA receptor dependent non-linearities are typically thought of as unique features of cortical pyramidal neurons that support to the computational power of these high-level microcircuits. Nevertheless, multiplicative integration of sound localization cues has been observed in single neurons of barn owl IC (Peña and Konishi, 2001; 2002), and the NMDA receptor dependent non-linearity we observe is comparable in magnitude to that reported during clustered activation of neighboring synapses in CA1 neurons (Harnett et al., 2012). Together, these data suggest that cooperative interactions between temporally correlated inputs may be a common neuronal operation throughout the central nervous system. An important distinction however is that most, if not all excitatory synapses in pyramidal neurons reside on dendritic spines; this compartmentalization greatly limits any cooperative interactions to neighboring synaptic inputs on the same branch (Gasparini and Magee, 2006; Losonczy and Magee, 2006). By contrast, auditory cortico-collicular axons often form large (~5 μm^3) synapses on the soma of dorsal IC neurons (Song et al., 2018). Depending on the impedance mismatch between the somatic and dendritic compartments, synaptic depolarizations at the soma could propagate passively throughout the neuron's multiple dendrites, thereby enabling cortical signals to non-linearly control ascending information irrespective of the spatial relationship of co-active inputs. However, further studies are necessary to identify the precise anatomical relationship between ascending and descending synapses in single IC neurons. Finally, we did not observe any overt correlation between the strength of descending EPSPs and the diverse biophysical properties of shell IC neurons. However, an important consideration is that our metrics of neuronal diversity perhaps do not reflect explicit cell-type categories in the IC. Future studies comparing descending transmission as a function of neurotransmitter phenotype (Naumov et al., 2019) or molecular markers (Goyer et al., 2019; Silveira et al., 2020; Kreeger et al., 2021), will likely provide more nuanced insight into the diversity of corticofugal control of the IC.

Implications for predictive control of tectal activity, synaptic plasticity, and perceptual learning.
The properties of corticofugal synapses could enable a context-dependent modulation of IC neurons across multiple timescales. Indeed, the rapid onset of descending EPSPs following cortical spikes (~5-8 ms) is more than twice as fast as sensory-evoked cortical gamma rhythms (30-50 Hz). Thus, descending signals could effectively synchronize neural ensembles across the ascending auditory hierarchy either to the temporal envelope of sound (Weible et al., 2020) or to internally generated rhythms. Alternatively, rapid auditory cortico-collicular transmission may be particularly advantageous in driving innate behaviors in response to sound. Indeed, auditory cortico-collicular neuron activity, either via optogenetic stimulation or loud sounds, directly triggers escape and flight behaviors in mice; these effects likely occur due via a descending activation of shell IC neurons projecting to the PAG (Xiong et al., 2015). As such, cortical signals could potentially trigger evolutionarily conserved motor programs to benefit survival.

We also found that descending synapses sustained transmission and drove tonic depolarizations even during seconds-long activity patterns, such that IC neurons may also integrate slower cortical state fluctuations. Intriguingly, auditory cortical neurons in behaving animals show enhanced firing rates during the delay period of auditory working memory tasks (Gottlieb et al., 1989) which apparently, precedes similar activity patterns in prefrontal cortex (Huang et al., 2016). If these working memory related neuronal ensembles include auditory cortico-collicular neurons, sustained transmission from descending synapses could cause seconds-long increases in IC neuron excitability based on working memory content. Accordingly, persistent delay period activity is observed in ~10% of IC neurons when rats engaged in an auditory working memory task (Sakurai, 1990), although future studies are necessary to determine the extent to which this activity is inherited from descending auditory cortical pathways.

Several studies now show that layer 5 corticofugal pyramidal neurons are necessary for perceptual learning in multiple different sensory tasks. Optogenetic inhibition of layer 5 pyramidal neurons in somatosensory cortex prevents behavioral adaptation following cue-related changes in a tactile detection task, although the same manipulation had no effect on touch perception (Ranganathan et al., 2018). Similarly, lesioning visual corticostriatal neurons prevents acquisition, but not performance of a visual detection task (Ruediger and Scanziani, 2020). In the auditory system, chemical lesions of auditory cortico-collicular neurons prevent the experience-dependent recovery of sound localization following monaural hearing loss (Bajo et al., 2010), although auditory cortex becomes dispensable once animals have learned to localize sounds using monaural cues (Bajo et al., 2019). Thus, although necessary for perceptual learning, corticofugal synapses may not be the primary locus of experience-dependent plasticity. Indeed, classic studies in barn owls suggest that ascending central IC -> external (shell) IC synapses are the first site of experience-dependent, spatial map plasticity in the auditory system (Brainard and Knudsen, 1993). In tandem with our current study, these results suggest that auditory cortico-collicular synapses' contributions to perceptual learning may not lie in their explicit ability to undergo classical Hebbian associative plasticity, but rather as permissive forces of heterosynaptic plasticity at ascending synapses.

Methods

Surgery for viral injections: All experiments were approved by the University of Michigan's IACUC and performed in accordance with NIH's Guide for the care and use of laboratory animals. All surgical procedures were performed under aseptic conditions. Surgeries were performed on 4-7 week old male or female C57BL6/J mice purchased from Jackson Labs or offspring of CBA x C57BL6/J matings bred in house for electrophysiology experiments. For the transsynaptic labeling experiments of Figure 1 – Figure Supplement 2, we used 6-8 week old Ai14 fl/fl mice bred in house (Jackson Labs stock #007914). Mice were deeply anesthetized with 4-5% isoflurane vaporized in O_2 and mounted in a rotating stereotaxic frame (model 1430, David Kopf Instruments). Isoflurane was subsequently lowered to 1-2% to maintain a deep anesthetic plane, as assessed by the absence of paw withdrawal reflex and stable respiration (1-1.5 breaths/s). Body temperature was maintained near 37-38° C using a feedback controlled, homeothermic heating blanket (Harvard

Apparatus). Mice were administered 5 mg/kg carprofen after induction as a pre-surgical analgesic. The scalp was clear of hair, swabbed with betadine, and a small incision was made in the skin overlying the left hemisphere. Topical 2% lidocaine was then applied to the wound margins. The stereotaxic frame was rotated ~50 degrees, allowing a vertical approach perpendicular to the layers of auditory cortex. A 200-400 μm craniotomy was carefully opened over the left auditory cortex (-2.75 mm from Bregma, centered on the lateral ridge) using a 0.5 mm diameter dental burr (19007-05, Fine Science Tools) and Foredom microdrill. The skull was frequently irrigated with chilled phosphate buffered saline (PBS) to prevent overheating during drilling. Following the craniotomy, a glass pipette (0.1-0.2 mm diameter at the tip) containing the pAAV-Syn-Chronos-GFP (Addgene #59170-AAV1) or AAV1-hSyn-Cre (Addgene #105553-AAV1) virus penetrated the auditory cortex at a rate of <10 μm/s using a motorized micromanipulator. A total of 100-200 nL virus was injected at 2-4 sites 810 and 710 μm below the pial surface (25-50 nL per site). Following injections, the pipette was maintained in place for an additional 5 min before slowly retracting at a rate of <10 μm/s. At the end of the surgery, the craniotomy was filled with bone wax, the skin was sutured, and the mouse was removed from the stereotax. Immediately following surgery, mice were given an analgesic injection of buprenorphine (0.03 mg/kg, s.c.) and allowed to recover on a heating pad before returning to their home cage. An additional post-operative dose of carprofen was administered 24 hours following surgery.

In vivo electrophysiology: 2-4 weeks following viral injections, mice were deeply anesthetized with isoflurane and mounted in a stereotax as described above. The skin overlying the skull was removed, the left temporal muscle was retracted, the stereotax was rotated ~50 degrees, and a 2-2.5 mm craniotomy was carefully opened over the left auditory cortex. For optogenetic stimulation in Figure 1, the dura overlying the auditory cortex was left intact and a cranial window was implanted over the exposed brain with cyanoacrylate glue and dental cement. For the electrical stimulation experiments in Figure 7, a small slit was carefully made in the dura and the craniotomy was subsequently sealed with silicone elastomer. The stereotaxic frame was returned to the horizontal position and a custom titanium headbar was affixed to the skull with dental cement. A 300-500 μm craniotomy was opened over the left IC and filled with a silicone elastomer plug. The mouse was then removed from the stereotax, anesthetized with urethane (1.5 g/kg, i.p.), and head-fixed in a custom-made sound attenuation chamber. Body temperature during the experiment was maintained at 37-38° C with a custom designed, feedback-controlled heating blanket. For optogenetic stimulation, a 0.5 NA, 400 μm core optic fiber (Thorlabs M45L02) coupled to a 470 nm LED (Thorlabs M470F3) was mounted on a micromanipulator and positioned <1 mm away from the auditory cortex cranial window. For electrical stimulation experiments, the silicone plug over auditory cortex was removed and a bipolar platinum-iridium electrode (FHC 30210) was carefully inserted ~800 μm into auditory cortex at an angle roughly perpendicular to the cortical layers. Electrical stimuli were delivered via a custom stimulus isolator designed in house. Sound clicks (0.2 ms duration) were presented at ~91 dB peak equivalent SPL via a free-field speaker (Peerless XT25SC90-04) positioned ~10 cm from the mouse's right ear. For whole-cell recordings, the silicone plug over the IC was removed and patch-clamp recordings were obtained from IC neurons via the "blind patch" approach using pipettes filled with K^+-rich internal solution containing (in mM): 115 K-Gluconate, 4 KCl, 0.1 EGTA, 10 HEPES, 14 Tris-Phosphocreatine, 4 Mg-ATP, 0.5 Tris-GTP, 4 NaCl, pH 7.2-7.3, 290 mOsm (open tip resistance: 5-10 MΩ). Data were acquired using an AM

Systems model 2400 patch-clamp amplifier, online filtered at 2-10 kHz, and digitized at 50 kHz with a National Instruments PCI-6343 card + BNC2090A interface controlled by Matlab based acquisition software (Wavesurfer). Data were recorded with the amplifier's pipette capacitance neutralization circuitry activated. Series resistance was typically between 20-60 MΩ. Field potentials in Figure 7 – Figure Supplement 1 were recorded with saline filled glass pipettes lowered 200-250 μm into the IC.

Auditory cortical inactivation by cooling: We built battery operated, constant current driven thermo-electric cooling devices designed around a small peltier module (NL1020T-01AC, Marlow Industries). The hot side of the peltier chip was mounted to a 6.35 mm diameter copper rod (length: ~76 mm) using thermally conductive adhesive. Fin type heatsinks were mounted to the copper rod. A machined blunt copper pin (3 mm at the base, 2 mm at the tip) was mounted on the cold side using the same adhesive and made contact with the dura mater over the auditory cortices. We performed control experiments in anesthetized mice (n = 5 cooling attempts in N = 4 mice) to verify that our devices effectively cooled the auditory cortices while minimally affecting the IC (Δtemperature in IC during cortical cooling = -1.9 ± 0.6° C). The settings used during our recordings bilaterally reduced the temperature of deep cortical layers to 14-17° C, which suffices to largely abolish auditory cortical activity (Lomber et al., 1999; Coomber et al., 2011; Anderson and Malmierca, 2013).

We used 8-12 week old C57Bl6/J mice for these experiments. Awake mice were handled for 3-5 days prior to recording and acclimated to head fixation while sitting comfortably in a Plexiglas tube. Following acclimation, mice were anesthetized, a ~0.5 mm craniotomy was opened over the left IC, and 2 mm craniotomies were opened over the left and right auditory cortices. The craniotomies were sealed with silicone elastomer and the mouse was allowed to recover for ~2 hours prior to recording. For recording, the silicone plugs were removed, the copper pin of the peltier devices were positioned in contact with the left and right auditory cortices, and the craniotomies were covered with 3-4% agar in saline. A saline filled glass electrode (~1-2 MOhm open tip resistance) was lowered into the superficial IC (~200 μm from surface) to record click-evoked field potentials and multi-unit clusters before, during, and after cooling of auditory cortices. After the recording, the craniotomies were sealed with silicone and the mouse was returned to its homecage. Each subject underwent 1-3 recording sessions.

In vitro electrophysiology: 2-4 weeks following viral injections, mice were deeply anesthetized with isoflurane, swiftly decapitated, and the brains carefully removed in warm (~34° C), oxygenated ACSF containing (in mM): 119 NaCl, 25 $NaHCO_3$, 3 KCl, 1.25 NaH_2PO_4, 15 glucose, 1 $MgCl_2$, 1.3 $CaCl_2$, 1 ascorbate, 3 pyruvate. 200-300 μm thick coronal slices of the IC were prepared with a vibratome (Campden Instruments). On each slice, a small cut was made in the lateral portion of the right cerebellum or right IC to aid with visual identification of the un-injected hemisphere. Slices were then incubated at 34° C in a holding chamber filled ACSF for 25-30 min and subsequently stored at room temperature. Experiments were generally performed within 3-4 hours following slice preparation. Following incubation, a slice was transferred to a recording chamber and held in place with single strands of unwaxed dental floss tightly strung around a platinum "harp". The slice was continuously perfused with oxygenated ACSF heated to 32-34° C (2-4 mL/min; chamber volume: ~

1 mL). 2-5 μM SR95531 was added to the ACSF to block $GABA_A$ receptors in most experiments of Figure 5C-H, Figure 6, Figure 6 – Figure Supplement 1, Figure 8, all voltage-clamp experiments, and some experiments of Figure 1. Neurons in the dorso-medial shell IC were visualized via DIC or Dodt contrast optics using a 40x or 63x objective (Zeiss Axioskop 2 FS Plus or Olympus BXW51 microscope). Neurons were targeted for whole-cell current-clamp recordings with pipettes filled with the same K^+-rich internal solution used for *in vivo* recordings (open tip resistance: 3-6 MΩ). For whole-cell voltage clamp experiments in Supplemental Figure 3, EPSCs were recorded at holding potentials between -60 and -70 mV with our standard K^+ internal solution or a Cs^+ based solution containing (in mM): 110 Cesium Methanesulfonate, 10 QX-314-Bromide, 0.1 EGTA, 10 HEPES, 0.5 Tris-GTP, 4.5 MgATP, 5 TEA-Cl, 10 Tris-phosphocreatine. Voltage-clamp experiments requiring positive holding potentials were exclusively performed using the Cs^+ based recipe. In some experiments, 30 μM Alexa 594 or 0.1% biocytin were added to the internal solution to visualize neuronal morphology via online fluorescence or post-hoc histological reconstruction.

Data were acquired with a Multiclamp 700B or AM System model 2400 amplifier, online filtered at 2-10 kHz, and digitized at 50 kHz with a National Instruments PCI-6343 card + BNC2090A interface controlled by Wavesurfer. In current clamp, pipette capacitance neutralization was employed and bridge balance was maintained (series resistance typically 10-30 MΩ). In a few instances, a small amount of negative bias current (-5 to -50 pA) was injected to hyperpolarize neurons and prevent spike initiation during optogenetic activation of cortico-collicular synapses. Series resistance compensation was employed in voltage clamp experiments (60-80%, bandwidth: 3 kHz). For dual pathway experiments, the central IC was electrically stimulated using an AM systems model 2100 stimulus isolator delivering mono- or bi-phasic shocks to a theta glass bipolar electrode placed ~500 μm from the recorded neuron. In these experiments, we made an effort to titrate the stimulation strength such that separate and combined pathway stimulation did not elicit spikes on most trials. Drugs were obtained from Tocris or HelloBio, aliquoted as stock solutions in distilled water, and stored at -20 C until the day of the experiment.

Data analysis: Electrophysiology data were analyzed using custom Matlab scripts. EPSP analyses were performed on averages of multiple trials (typically >10 trials per condition) after baseline membrane potential subtraction and lowpass filtering at 1 kHz unless explicitly noted in the text. Peak amplitudes of single EPSPs were calculated by averaging data points ±0.1 ms around the local maximum following optogenetic stimulation Halfwidths are calculated as the full width at half-maximum of the peak. EPSP onset latency was defined as the time following optogenetic stimulus onset when the membrane potential reaches 20% of peak. The tonic EPSP amplitude during 20 Hz trains was calculated as follows: We first linearly interpolated the membrane potential data between each light flash to remove the phasic EPSP component. The trace was then smoothed using a 50 ms sliding window. Datapoints during the final 1s period of the stimulus train were then averaged to estimate the amplitude of tonic membrane potential change. In certain experiments of Figures 4, 7, and 8, train stimuli and click sounds occasionally triggered APs in IC neurons both *in vivo* and *in vitro*. In these cases, APs were digitally removed prior to averaging the traces by linearly interpolating 0.1-0.2 ms of datapoints after the membrane potential crossed spike threshold (~20 mV/ms). Shock artifacts during electrical stimulation experiments were similarly removed via linear

705 interpolation. In summary plots, black symbols are individual cells, magenta is mean ± SEM, and
706 lines connect data from the same recording unless otherwise stated.
707
708 The expected linear waveforms for temporal summation experiments were calculated as follows.
709 The average waveform of a single optogenetically evoked EPSP was peak normalized to the first
710 EPSP in the recorded 20 or 50 Hz train from the same cell. We subsequently convolved the single
711 EPSP waveform with a 20 or 50 Hz binary pulse train using the Matlab function convr(). We then
712 calculated the peak amplitude ratios for each EPSP in observed and expected trains.
713
714 For the free-field sound presentation experiments of Figure 7D-E, we limited our analyses to
715 superficial IC neurons that showed onset EPSPs in response to clicks. Other IC neurons
716 encountered during these experiments showed either sound-evoked IPSPs (n=7 cells from N=5
717 mice) or IPSPs followed by rebound depolarizations (n=6 cells from N=5 mice); analyses of these
718 data will be presented in a separate report. Click-evoked field potentials in Figure 7 – Figure
719 Supplement 1 and 2 were analyzed after baseline subtraction and low-pass filtering the records at
720 500 Hz. Multi-unit activity was detected as threshold crossings after applying a bandpass filter
721 (between 300 Hz and 5 kHz) to the recordings. Peristimulus time histograms (PSTHs) of spike
722 activity were generated with 100 μs bin-widths and smoothed with a 2 ms sliding window. Onset
723 latencies of field potentials and multi-unit PSTHs were defined as the time following click onset at
724 which the data reached 20% of its peak. Average LFP waveforms and PSTHs were composed of
725 300-302 trials per condition.
726
727 In dual pathway experiments of Figure 8, the onset latency of ascending and descending EPSPs
728 varied across cells. Thus, the relative timing of electrical and optogenetic stimulation during
729 combined pathway activation was calculated online and on a cell-by-cell basis, such that the onset
730 of descending auditory cortical EPSPs collided with the peak of ascending EPSPs from central IC
731 as predicted from our *in vivo* latency measurements (Figure 7; range of Δt between stimulation of
732 descending and ascending synapses: -1.3 to 16.4 ms). These stimulation parameters were held
733 constant across control and R-CPP conditions for each cell. The expected linear summation was
734 calculated by digitally summing the average synaptic waveforms following stimulation of either
735 pathway alone, accounting for the temporal offset employed during synchronous pathway
736 activation.
737
738 *Histology and Confocal Imaging:* Mice were deeply anesthetized in a glass induction chamber
739 circulated with 4.2 mL isoflurane and transcardially perfused with ~80-100 mL of PBS followed by
740 ~80-100 mL of 10% buffered formalin (Fisher Scientific catalog # 23-245684). Brains were carefully
741 removed, stored in 10% formalin and protected from light for 24 hours. Subsequently, brains were
742 stored in PBS for up to 72 hours and 100 μm thick coronal slices were cut using a ceramic blade
743 (Cadence Endurium) and a Leica VT1000s vibratome, mounted onto slides and coverslipped using
744 Fluoromount, then protected from light and allowed to dry at room temperature for ~12-24 hours.
745 Slides were then stored at 4 C until ready for use. Images were collected using a Leica TCS SP8
746 laser scanning confocal microscope equipped with a 10x objective.
747

Statistics: Although not explicitly pre-determined prior to data collection, sample sizes reflect commonly accepted standards in the field. Data were tested for normality using a Lilliefors test prior to statistical comparisons. Parametric, two-tailed t-tests are employed for normally distributed data. Non-parametric rank-sum or sign-rank tests are used when one or more of the distributions deviate from normal. Alpha is corrected for multiple comparisons in post-hoc significance tests following ANOVA. Statistics were run in Matlab or Graphpad Prism 9.

Conflict of Interest Statement: The authors declare no conflicts.

Acknowledgments: Funding was generously provided by the Whitehall Foundation, Hearing Health Foundation, and NIH/NIDCD R01DC019090 to PFA, as well as T32 DC005356 and T32 DC000011 pre-doctoral awards to HMO. We thank Drs. Michael Roberts, Marina Silveira, Gunnar Quass and Meike Rogalla for critical comments on the manuscript.

References

Abbott LF, Varela JA, Sen K, Nelson SB (1997) Synaptic depression and cortical gain control. Science 275:220–224.

Ahuja TK, Wu SH (2007) Intrinsic membrane properties and synaptic response characteristics of neurons in the rat's external cortex of the inferior colliculus. Neuroscience 145:851–865.

Anderson LA, Malmierca MS (2013) The effect of auditory cortex deactivation on stimulus-specific adaptation in the inferior colliculus of the rat. Eur J Neurosci 37:52–62.

Apostolides PF, Trussell LO (2014) Control of interneuron firing by subthreshold synaptic potentials in principal cells of the dorsal cochlear nucleus. Neuron 83:324–330.

Arnth-Jensen N, Jabaudon D, Scanziani M (2002) Cooperation between independent hippocampal synapses is controlled by glutamate uptake. Nat Neurosci 5:325–331.

Ayala YA, Udeh A, Dutta K, Bishop D, Malmierca MS, Oliver DL (2015) Differences in the strength of cortical and brainstem inputs to SSA and non-SSA neurons in the inferior colliculus. Sci Rep 5:10383.

Bajo VM, Nodal FR, Korn C, Constantinescu AO, Mann EO, Boyden ES, King AJ (2019) Silencing cortical activity during sound-localization training impairs auditory perceptual learning. Nat Commun 10:3075.

Bajo VM, Nodal FR, Moore DR, King AJ (2010) The descending corticocollicular pathway mediates learning-induced auditory plasticity. Nat Neurosci 13:253–260.

Barnstedt O, Keating P, Weissenberger Y, King AJ, Dahmen JC (2015) Functional Microarchitecture of the Mouse Dorsal Inferior Colliculus Revealed through In Vivo Two-Photon Calcium Imaging. J Neurosci 35:10927–10939.

Bertero A, Garcia C, Apicella AJ (2021) Corticofugal VIP Gabaergic Projection Neurons in the Mouse Auditory and Motor Cortex. Front Neural Circuits 15:714780.

Blackwell JM, Lesicko AM, Rao W, De Biasi M, Geffen MN (2020) Auditory cortex shapes sound responses in the inferior colliculus. eLife 9:e51890.

Bordi F, LeDoux JE (1994) Response properties of single units in areas of rat auditory thalamus that project to the amygdala: II. Cells receiving convergent auditory and somatosensory inputs and cells antidromically activated by amygdala stimulation. Exp Brain Res 98:275–286.

Brainard MS, Knudsen EI (1993) Experience-dependent plasticity in the inferior colliculus: a site for visual calibration of the neural representation of auditory space in the barn owl. J Neurosci Off J Soc Neurosci 13:4589–4608.

Branco T, Clark BA, Häusser M (2010) Dendritic discrimination of temporal input sequences in cortical neurons. Science 329:1671–1675.

Brown SP, Hestrin S (2009) Intracortical circuits of pyramidal neurons reflect their long-range axonal targets. Nature 457:1133–1136.

Cai D, Yue Y, Su X, Liu M, Wang Y, You L, Xie F, Deng F, Chen F, Luo M, Yuan K (2019) Distinct Anatomical Connectivity Patterns Differentiate Subdivisions of the Nonlemniscal Auditory Thalamus in Mice. Cereb Cortex 29:2437–2454.

Champoux F, Paiement P, Mercier C, Lepore F, Lassonde M, Gagné J-P (2007) Auditory processing in a patient with a unilateral lesion of the inferior colliculus: Role of the inferior colliculus in humans. Eur J Neurosci 25:291–297.

Chen C, Cheng M, Ito T, Song S (2018) Neuronal Organization in the Inferior Colliculus Revisited with Cell-Type-Dependent Monosynaptic Tracing. J Neurosci 38:3318–3332.

Clements JD, Lester RA, Tong G, Jahr CE, Westbrook GL (1992) The time course of glutamate in the synaptic cleft. Science 258:1498–1501.

Coomber B, Edwards D, Jones SJ, Shackleton TM, Goldschmidt J, Wallace MN, Palmer AR (2011) Cortical inactivation by cooling in small animals. Front Syst Neurosci 5:53.

Coomes DL, Schofield BR (2004) Projections from the auditory cortex to the superior olivary complex in guinea pigs. Eur J Neurosci 19:2188–2200.

Destexhe A, Rudolph M, Paré D (2003) The high-conductance state of neocortical neurons in vivo. Nat Rev Neurosci 4:739–751.

Diamond IT, Jones EG, Powell TPS (1969) The projection of the auditory cortex upon the diencephalon and brain stem in the cat. Brain Res 15:305–340.

Doucet JR, Molavi DL, Ryugo DK (2003) The source of corticocollicular and corticobulbar projections in area Te1 of the rat. Exp Brain Res 153:461–466.

Faye-Lund H, Osen KK (1985) Anatomy of the inferior colliculus in rat. Anat Embryol (Berl) 171:1–20.

Feldman DE, Brainard MS, Knudsen EI (1996) Newly learned auditory responses mediated by NMDA receptors in the owl inferior colliculus. Science 271:525–528.

Feng B, Morley RM, Jane DE, Monaghan DT (2005) The effect of competitive antagonist chain length on NMDA receptor subunit selectivity. Neuropharmacology 48:354–359.

Fletcher LN, Williams SR (2019) Neocortical Topology Governs the Dendritic Integrative Capacity of Layer 5 Pyramidal Neurons. Neuron 101:76-90.e4.

Gasparini S, Magee JC (2006) State-dependent dendritic computation in hippocampal CA1 pyramidal neurons. J Neurosci Off J Soc Neurosci 26:2088–2100.

Geis H-RAP, van der Heijden M, Borst JGG (2011) Subcortical input heterogeneity in the mouse inferior colliculus. J Physiol 589:3955–3967.

Gottlieb Y, Vaadia E, Abeles M (1989) Single unit activity in the auditory cortex of a monkey performing a short term memory task. Exp Brain Res 74:139–148.

Goyer D, Silveira MA, George AP, Beebe NL, Edelbrock RM, Malinski PT, Schofield BR, Roberts MT (2019) A novel class of inferior colliculus principal neurons labeled in vasoactive intestinal peptide-Cre mice. eLife 8:e43770.

Harnett MT, Makara JK, Spruston N, Kath WL, Magee JC (2012) Synaptic amplification by dendritic spines enhances input cooperativity. Nature 491:599–602.

Hsu C-L, Zhao X, Milstein AD, Spruston N (2018) Persistent Sodium Current Mediates the Steep Voltage Dependence of Spatial Coding in Hippocampal Pyramidal Neurons. Neuron 99:147-162.e8.

Huang Y, Matysiak A, Heil P, König R, Brosch M (2016) Persistent neural activity in auditory cortex is related to auditory working memory in humans and nonhuman primates. eLife 5.

Hurley LM, Pollak GD (2005) Serotonin shifts first-spike latencies of inferior colliculus neurons. J Neurosci Off J Soc Neurosci 25:7876–7886.

Isaacson JS, Solís JM, Nicoll RA (1993) Local and diffuse synaptic actions of GABA in the hippocampus. Neuron 10:165–175.

Joswig H, Schönenberger U, Brügge D, Richter H, Surbeck W (2015) Reversible pure word deafness due to inferior colliculi compression by a pineal germinoma in a young adult. Clin Neurol Neurosurg 139:62–65.

Kitagawa M, Sakaba T (2019) Developmental changes in the excitatory short-term plasticity at input synapses in the rat inferior colliculus. Eur J Neurosci 50:2830–2846.

Kole MHP, Letzkus JJ, Stuart GJ (2007) Axon initial segment Kv1 channels control axonal action potential waveform and synaptic efficacy. Neuron 55:633–647.

Kong L, Xiong C, Li L, Yan J (2014) Frequency-specific corticofugal modulation of the dorsal cochlear nucleus in mice. Front Syst Neurosci 8 Available at: http://journal.frontiersin.org/article/10.3389/fnsys.2014.00125/abstract [Accessed November 16, 2020].

859 Kreeger LJ, Connelly CJ, Mehta P, Zemelman BV, Golding NL (2021) Excitatory cholecystokinin
860 neurons of the midbrain integrate diverse temporal responses and drive auditory thalamic
861 subdomains. Proc Natl Acad Sci U S A 118:e2007724118.

862 Krishna BS, Semple MN (2000) Auditory Temporal Processing: Responses to Sinusoidally
863 Amplitude-Modulated Tones in the Inferior Colliculus. J Neurophysiol 84:255–273.

864 LeDoux J, Farb C, Ruggiero D (1990) Topographic organization of neurons in the acoustic
865 thalamus that project to the amygdala. J Neurosci 10:1043–1054.

866 Lefort S, Tomm C, Floyd Sarria J-C, Petersen CCH (2009) The excitatory neuronal network of the
867 C2 barrel column in mouse primary somatosensory cortex. Neuron 61:301–316.

868 Lesicko AMH, Hristova TS, Maigler KC, Llano DA (2016) Connectional Modularity of Top-Down and
869 Bottom-Up Multimodal Inputs to the Lateral Cortex of the Mouse Inferior Colliculus. J
870 Neurosci 36:11037–11050.

871 Lester RA, Jahr CE (1992) NMDA channel behavior depends on agonist affinity. J Neurosci Off J
872 Soc Neurosci 12:635–643.

873 Llano DA, Slater BJ, Lesicko AMH, Stebbings KA (2014) An auditory colliculothalamocortical brain
874 slice preparation in mouse. J Neurophysiol 111:197–207.

875 Loftus WC, Malmierca MS, Bishop DC, Oliver DL (2008) The cytoarchitecture of the inferior
876 colliculus revisited: A common organization of the lateral cortex in rat and cat. Neuroscience
877 154:196–205.

878 Lomber SG, Payne BR, Horel JA (1999) The cryoloop: an adaptable reversible cooling deactivation
879 method for behavioral or electrophysiological assessment of neural function. J Neurosci
880 Methods 86:179–194.

881 Losonczy A, Magee JC (2006) Integrative properties of radial oblique dendrites in hippocampal
882 CA1 pyramidal neurons. Neuron 50:291–307.

883 Lumani A, Zhang H (2010) Responses of neurons in the rat's dorsal cortex of the inferior colliculus
884 to monaural tone bursts. Brain Res 1351:115–129.

885 Ma CL, Kelly JB, Wu SH (2002) AMPA and NMDA receptors mediate synaptic excitation in the rat's
886 inferior colliculus. Hear Res 168:25–34.

887 Markram H, Wang Y, Tsodyks M (1998) Differential signaling via the same axon of neocortical
888 pyramidal neurons. Proc Natl Acad Sci U S A 95:5323–5328.

889 Massopust LC, Ordy JM (1962) Auditory organization of the inferior colliculi in the cat. Exp Neurol
890 6:465–477.

891 Masterton RB, Jane JA, Diamond IT (1968) Role of brain-stem auditory structures in sound
892 localization. II. Inferior colliculus and its brachium. J Neurophysiol 31:96–108.

893 Mellott JG, Foster NL, Ohl AP, Schofield BR (2014) Excitatory and inhibitory projections in parallel
894 pathways from the inferior colliculus to the auditory thalamus. Front Neuroanat 8 Available

at: http://journal.frontiersin.org/article/10.3389/fnana.2014.00124/abstract [Accessed July 24, 2020].

Mitani A, Shimokouchi M, Nomura S (1983) Effects of stimulation of the primary auditory cortex upon colliculogeniculate neurons in the inferior colliculus of the cat. Neurosci Lett 42:185–189.

Moore LA, Trussell LO (2017) Corelease of Inhibitory Neurotransmitters in the Mouse Auditory Midbrain. J Neurosci Off J Soc Neurosci 37:9453–9464.

Nakamoto KT, Jones SJ, Palmer AR (2008) Descending projections from auditory cortex modulate sensitivity in the midbrain to cues for spatial position. J Neurophysiol 99:2347–2356.

Nakamoto KT, Shackleton TM, Palmer AR (2010) Responses in the inferior colliculus of the guinea pig to concurrent harmonic series and the effect of inactivation of descending controls. J Neurophysiol 103:2050–2061.

Naumov V, Heyd J, de Arnal F, Koch U (2019) Analysis of excitatory and inhibitory neuron types in the inferior colliculus based on Ih properties. J Neurophysiol 121:2126–2139.

Nwabueze-Ogbo FC, Popelár J, Syka J (2002) Changes in the acoustically evoked activity in the inferior colliculus of the rat after functional ablation of the auditory cortex. Physiol Res 51 Suppl 1:S95–S104.

O'Connor DH, Peron SP, Huber D, Svoboda K (2010) Neural activity in barrel cortex underlying vibrissa-based object localization in mice. Neuron 67:1048–1061.

Oliver DL (1984) Neuron types in the central nucleus of the inferior colliculus that project to the medial geniculate body. Neuroscience 11:409–424.

Oliver DL, Hall WC (1978) The medial geniculate body of the tree shrew,Tupaia glis I. Cytoarchitecture and midbrain connections. J Comp Neurol 182:423–458.

Peña JL, Konishi M (2001) Auditory spatial receptive fields created by multiplication. Science 292:249–252.

Pena JL, Konishi M (2002) From postsynaptic potentials to spikes in the genesis of auditory spatial receptive fields. J Neurosci Off J Soc Neurosci 22:5652–5658.

Peruzzi D, Sivaramakrishnan S, Oliver DL (2000) Identification of cell types in brain slices of the inferior colliculus. Neuroscience 101:403–416.

Polsky A, Mel B, Schiller J (2009) Encoding and decoding bursts by NMDA spikes in basal dendrites of layer 5 pyramidal neurons. J Neurosci Off J Soc Neurosci 29:11891–11903.

Ponvert ND, Jaramillo S (2019) Auditory Thalamostriatal and Corticostriatal Pathways Convey Complementary Information about Sound Features. J Neurosci 39:271–280.

Qi J, Zhang Z, He N, Liu X, Zhang C, Yan J (2020) Cortical Stimulation Induces Excitatory Postsynaptic Potentials of Inferior Colliculus Neurons in a Frequency-Specific Manner. Front Neural Circuits 14:591986.

Ranganathan GN, Apostolides PF, Harnett MT, Xu N-L, Druckmann S, Magee JC (2018) Active dendritic integration and mixed neocortical network representations during an adaptive sensing behavior. Nat Neurosci 21:1583–1590.

Ruediger S, Scanziani M (2020) Learning speed and detection sensitivity controlled by distinct cortico-fugal neurons in visual cortex. eLife 9.

Ryugo DK, Weinberger NM (1976) Corticofugal modulation of the medial geniculate body. Exp Neurol 51:377–391.

Sakurai Y (1990) Cells in the rat auditory system have sensory-delay correlates during the performance of an auditory working memory task. Behav Neurosci 104:856–868.

Saldaña E, Feliciano M, Mugnaini E (1996) Distribution of descending projections from primary auditory neocortex to inferior colliculus mimics the topography of intracollicular projections. J Comp Neurol 371:15–40.

Saldaña E, Merchán MA (1992) Intrinsic and commissural connections of the rat inferior colliculus. J Comp Neurol 319:417–437.

Schofield BR, Coomes DL, Schofield RM (2006) Cells in Auditory Cortex that Project to the Cochlear Nucleus in Guinea Pigs. J Assoc Res Otolaryngol 7:95–109.

Schwartz EJ, Rothman JS, Dugué GP, Diana M, Rousseau C, Silver RA, Dieudonné S (2012) NMDA receptors with incomplete Mg^{2+} block enable low-frequency transmission through the cerebellar cortex. J Neurosci Off J Soc Neurosci 32:6878–6893.

Silveira MA, Anair JD, Beebe NL, Mirjalili P, Schofield BR, Roberts MT (2020) Neuropeptide Y Expression Defines a Novel Class of GABAergic Projection Neuron in the Inferior Colliculus. J Neurosci 40:4685–4699.

Sinex DG, Li H (2007) Responses of Inferior Colliculus Neurons to Double Harmonic Tones. J Neurophysiol 98:3171–3184.

Smith PH (1992) Anatomy and physiology of multipolar cells in the rat inferior collicular cortex using the in vitro brain slice technique. J Neurosci Off J Soc Neurosci 12:3700–3715.

Song JH, Lucaci D, Calangiu I, Brown MTC, Park JS, Kim J, Brickley SG, Chadderton P (2018) Combining mGRASP and Optogenetics Enables High-Resolution Functional Mapping of Descending Cortical Projections. Cell Rep 24:1071–1080.

Stebbings KA, Lesicko AMH, Llano DA (2014) The auditory corticocollicular system: Molecular and circuit-level considerations. Hear Res 314:51–59.

Stoelzel CR, Bereshpolova Y, Alonso J-M, Swadlow HA (2017) Axonal Conduction Delays, Brain State, and Corticogeniculate Communication. J Neurosci Off J Soc Neurosci 37:6342–6358.

Stuart G, Sakmann B (1995) Amplification of EPSPs by axosomatic sodium channels in neocortical pyramidal neurons. Neuron 15:1065–1076.

Stuart GJ, Spruston N (2015) Dendritic integration: 60 years of progress. Nat Neurosci 18:1713–1721.

Sun H, Wu SH (2009) The physiological role of pre- and postsynaptic GABA(B) receptors in membrane excitability and synaptic transmission of neurons in the rat's dorsal cortex of the inferior colliculus. Neuroscience 160:198–211.

Suthakar K, Ryugo DK (2017) Descending projections from the inferior colliculus to medial olivocochlear efferents: Mice with normal hearing, early onset hearing loss, and congenital deafness. Hear Res 343:34–49.

Syka J, Popelár J, Kvasnák E, Astl J (2000) Response properties of neurons in the central nucleus and external and dorsal cortices of the inferior colliculus in guinea pig. Exp Brain Res 133:254–266.

Szabadics J, Tamás G, Soltesz I (2007) Different transmitter transients underlie presynaptic cell type specificity of GABAA,slow and GABAA,fast. Proc Natl Acad Sci U S A 104:14831–14836.

Takahashi H, Magee JC (2009) Pathway interactions and synaptic plasticity in the dendritic tuft regions of CA1 pyramidal neurons. Neuron 62:102–111.

Valdés-Baizabal C, Casado-Román L, Bartlett EL, Malmierca MS (2021) In vivo whole-cell recordings of stimulus-specific adaptation in the inferior colliculus. Hear Res 399:107978.

Vila C-H, Williamson RS, Hancock KE, Polley DB (2019) Optimizing optogenetic stimulation protocols in auditory corticofugal neurons based on closed-loop spike feedback. J Neural Eng 16:066023.

Weedman DL, Ryugo DK (1996) Projections from auditory cortex to the cochlear nucleus in rats: synapses on granule cell dendrites. J Comp Neurol 371:311–324.

Weible AP, Yavorska I, Wehr M (2020) A Cortico-Collicular Amplification Mechanism for Gap Detection. Cereb Cortex N Y N 1991 30:3590–3607.

Williamson RS, Polley DB (2019) Parallel pathways for sound processing and functional connectivity among layer 5 and 6 auditory corticofugal neurons. eLife 8:e42974.

Winer JA (2006) Decoding the auditory corticofugal systems. Hear Res 212:1–8.

Winer JA, Diehl JJ, Larue DT (2001) Projections of auditory cortex to the medial geniculate body of the cat. J Comp Neurol 430:27–55.

Winer JA, Larue DT, Diehl JJ, Hefti BJ (1998) Auditory cortical projections to the cat inferior colliculus. J Comp Neurol 400:147–174.

Wong AB, Borst JGG (2019) Tonotopic and non-auditory organization of the mouse dorsal inferior colliculus revealed by two-photon imaging. eLife 8:e49091.

Wu SH (2004) Contribution of AMPA, NMDA, and GABAA Receptors to Temporal Pattern of Postsynaptic Responses in the Inferior Colliculus of the Rat. J Neurosci 24:4625–4634.

Xiao Z, Suga N (2002) Modulation of cochlear hair cells by the auditory cortex in the mustached bat. Nat Neurosci 5:57–63.

1004 Xiong XR, Liang F, Zingg B, Ji X, Ibrahim LA, Tao HW, Zhang LI (2015) Auditory cortex controls
1005 sound-driven innate defense behaviour through corticofugal projections to inferior colliculus.
1006 Nat Commun 6:7224.

1007 Yan J, Suga N (1999) Corticofugal Amplification of Facilitative Auditory Responses of Subcortical
1008 Combination-Sensitive Neurons in the Mustached Bat. J Neurophysiol 81:817–824.

1009 Yan W, Suga N (1998) Corticofugal modulation of the midbrain frequency map in the bat auditory
1010 system. Nat Neurosci 1:54–58.

1011 Yavorska I, Wehr M (2021) Effects of Locomotion in Auditory Cortex Are Not Mediated by the VIP
1012 Network. Front Neural Circuits 15:618881.

1013 Yu Y-Q, Xiong Y, Chan Y-S, He J (2004) Corticofugal gating of auditory information in the
1014 thalamus: an in vivo intracellular recording study. J Neurosci Off J Soc Neurosci 24:3060–
1015 3069.

1016 Zingg B, Chou X-L, Zhang Z-G, Mesik L, Liang F, Tao HW, Zhang LI (2017) AAV-Mediated
1017 Anterograde Transsynaptic Tagging: Mapping Corticocollicular Input-Defined Neural
1018 Pathways for Defense Behaviors. Neuron 93:33–47.

1019 Zingg B, Peng B, Huang J, Tao HW, Zhang LI (2020) Synaptic Specificity and Application of
1020 Anterograde Transsynaptic AAV for Probing Neural Circuitry. J Neurosci Off J Soc Neurosci
1021 40:3250–3267.

1022 Zucker RS, Regehr WG (2002) Short-term synaptic plasticity. Annu Rev Physiol 64:355–405.

1023
1024

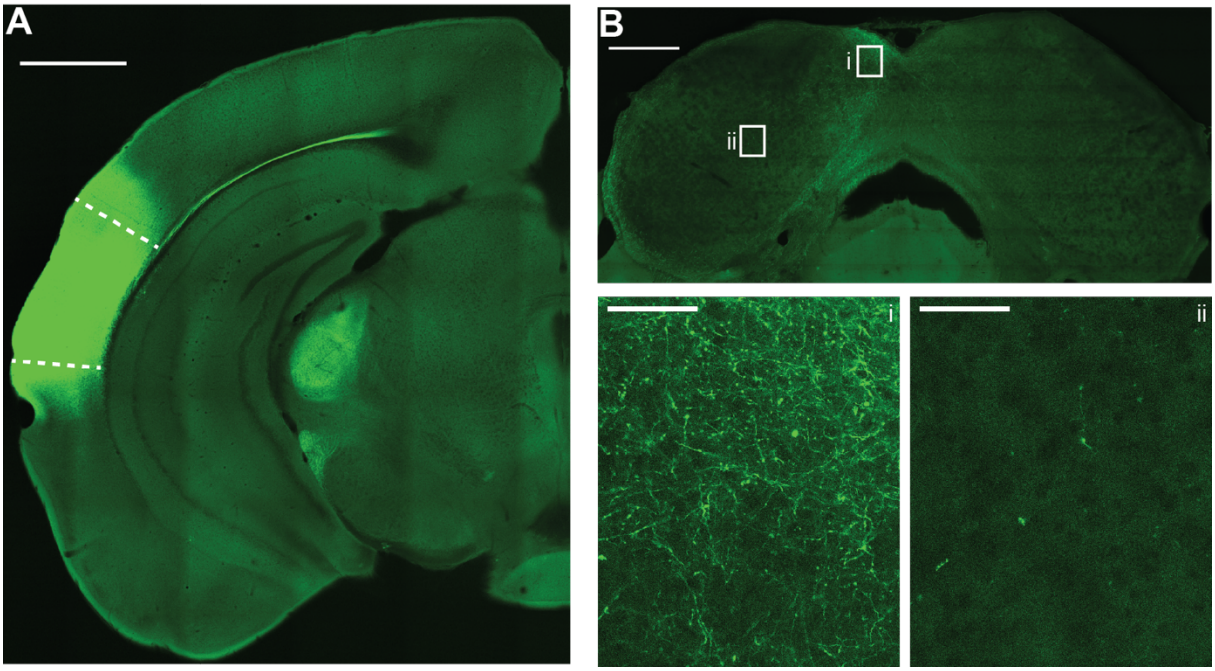

Figure 1 – Figure Supplement 1. *Auditory cortical axons are preferentially distributed in the non-lemniscal shell IC.*

A) Example micrograph of Chronos-GFP injection site in the left auditory cortex. Dashed lines denote approximate borders of auditory cortical areas as defined by Allen Brain Atlas. Scale bar = 1 mm. Of note is the strong corticofugal fiber labeling in medial geniculate body.

B) Micrograph of IC from the same case as in panel A. Scale bar = 500 µm. Rectangles denote areas of interest in the dorso-medial shell (i) or central (ii) IC shown at higher magnification below. Of note is the preferential distribution of GFP labeled axons in the shell regions, with comparatively sparse labeling in central IC. Scale bars for i and ii = 50 µm.

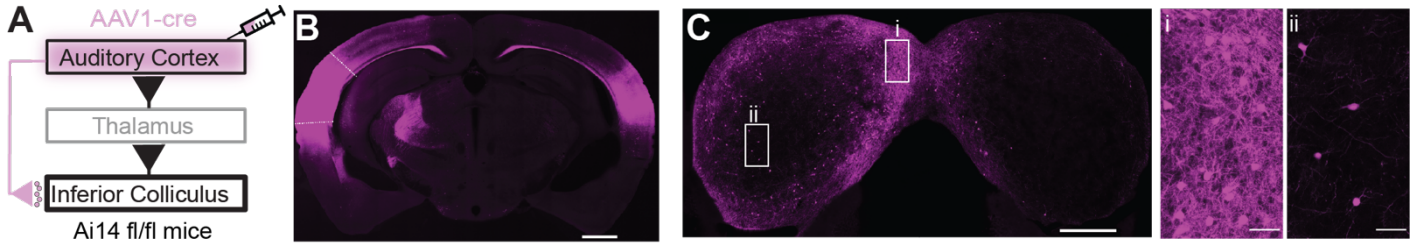

Figure 1 – Figure Supplement 2: *Anterograde trans-synaptic labeling of auditory cortical targets in the IC.*

A) Cartoon of experiment. An AAV1-cre virus is injected into the auditory cortex of tdTomato reporter mice (Ai14 fl/fl). This approach leads to anterograde trans-synaptic viral spread and thus tdTomato expression in postsynaptic neurons downstream of the injection site (Zingg et al., 2017;2020).

B) Micrograph of an example injection site showing viral diffusion throughout primary and secondary auditory fields. Dashed lines are approximate borders of auditory cortical areas. Scale Bar = 1 mm.

C) Micrograph of the IC from the same case as in B. Scale bar = 500 µm. Rectangles denote areas of interest in the shell (i) or central (ii) IC shown at higher magnification in the accompanying panels. Of note is the dense labeling of neuronal somata in the shell compared to the central IC. Scale bars = 50 µm.

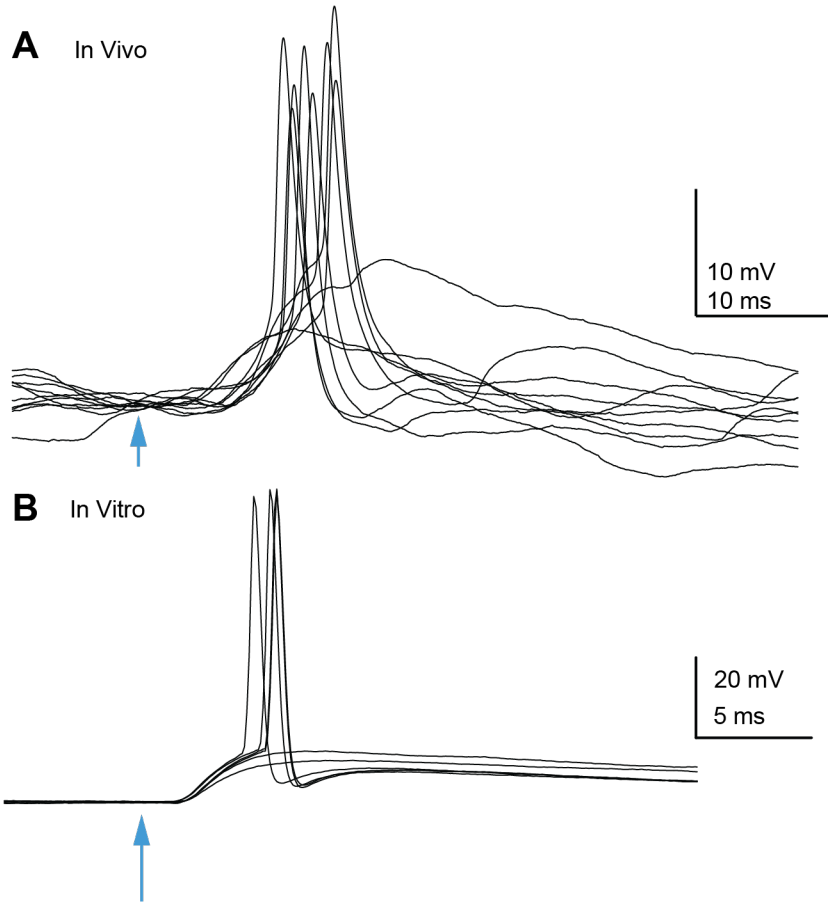

Figure 1 – Figure Supplement 3: *Auditory cortico-collicular EPSPs can trigger spikes in IC neurons in vivo and in vitro.*
A) Example overlaid trials from an *in vivo* whole-cell recording of a superficial IC neuron. Optogenetic stimulation of auditory cortex denoted by arrowhead.
B) Example trials from an *in vitro* recording.

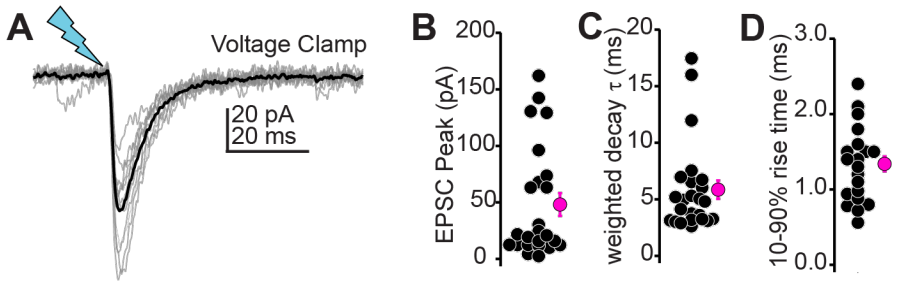

Figure 1 – Figure Supplement 4: *Auditory Cortico-collicular transmission in voltage-clamp.* **A)** Example EPSCs recorded in voltage clamp. Gray and black traces are individual trials and average, respectively. **B-D)** Summary data for EPSC peak amplitudes (B), decay time constant (C), and 10-90% rise time (D) in n=24 cells from N = 10 mice.

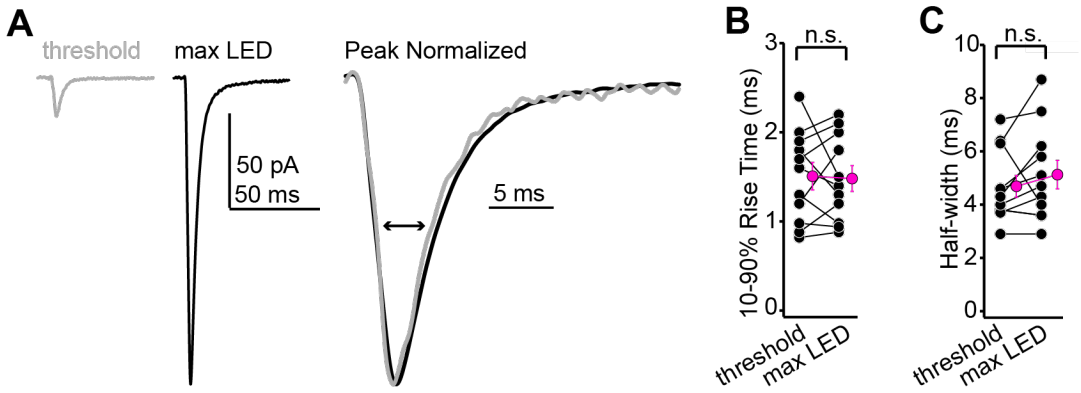

Figure 2 – Figure Supplement 1: *EPSC rise times and half-widths are similar across minimal and maximal stimulation intensities.*

A) Example averages of successful EPSCs recorded at threshold stimulation (gray) or at maximal LED intensity (black). Right shows the two waveforms scaled to peak and at a faster time base.

B) Group data showing that the EPSC rise time is similar at threshold and maximal stimulation intensities (n = 11 neurons from N = 4 mice. 1.5 ±0.2 vs. 1.5 ± 0.1 ms for threshold and maximal intensity, respectively. p = 0.85, paired t-test).

C) Same as B, but for EPSC halfwidths (n = 11 neurons from N = 4 mice. 4.7 ± 0.4 vs. 5.1 ± 0.5 ms, respectively. p = 0.14, sign-rank test).

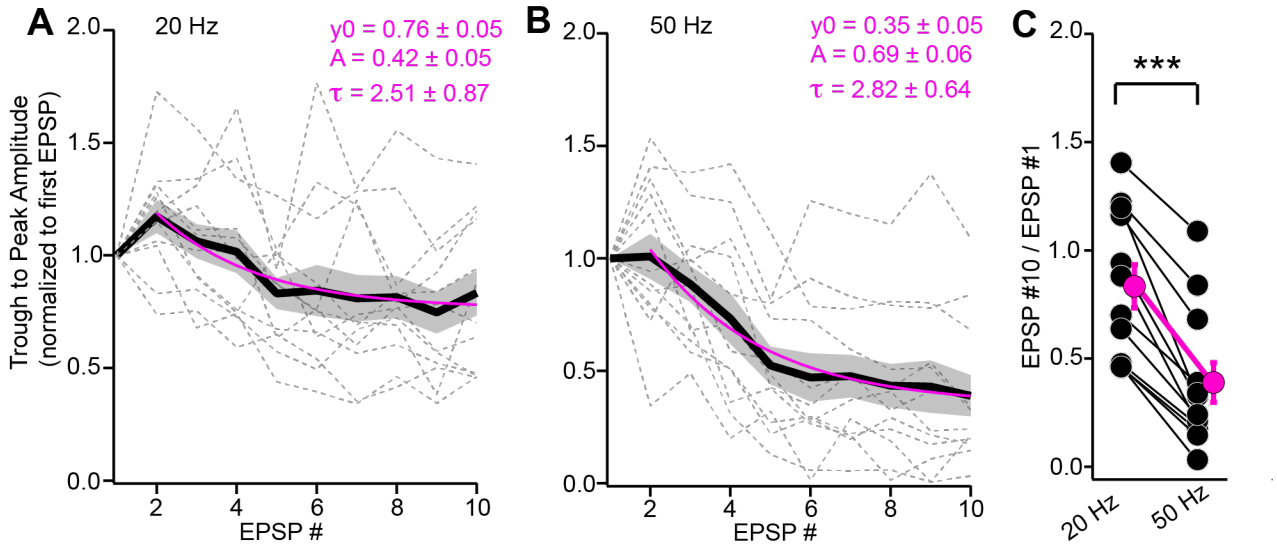

Figure 4 – Figure Supplement 1: *Depression of instantaneous EPSP amplitudes during trains.* **A,B)** The trough-to-peak amplitude of individual EPSPs (normalized to first EPSP) plotted as a function of stimulus # for 20 (A) and 50 Hz (B) trains. Data are from the same experiments as Figure 4A-D. Gray dotted lines are individual experiments; black + shading is mean ± SEM. Magenta lines are mono-exponential fits to the data beginning at the second stimulus. Fit parameters are provided above.
C) Summary data plotting the ratio of instantaneous amplitudes for the 10th and 1st EPSPs, indicating significantly greater depression of EPSP amplitudes during 50 Hz compared to 20 Hz stimulation.

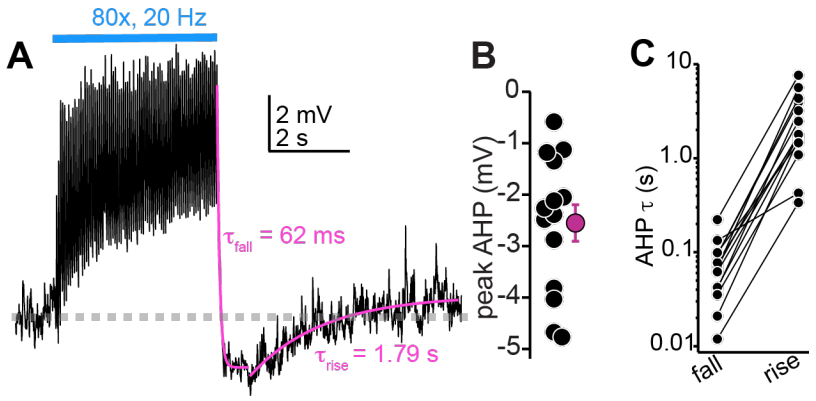

Figure 4 – Figure Supplement 2: *Large AHPs follow the cessation of auditory cortico-collicular activity in vivo.*

A) Membrane potential (average of multiple trials) during prolonged auditory cortical activity *in vivo*. Magenta are mono-exponential fits to the membrane potential fall and rise upon cessation of optogenetic stimulation.

B) Peak AHP amplitude (relative to baseline Vm) in n=14 cells.

C) Time constants for the fall and raise of the membrane potential for n = 14 cells. The data are on a log scale due to the order of magnitude difference in exponent values for fall and rise.

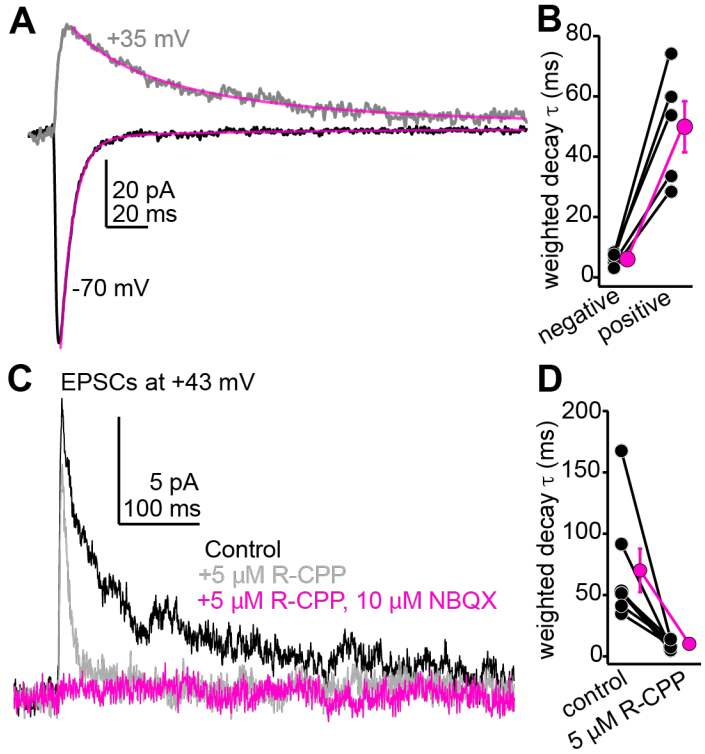

Figure 5 – Figure Supplement 1: *The slow component of auditory cortico-collicular EPSCs recorded at positive potentials is blocked by 5 μM R-CPP, consistent with the presence of R-CPP sensitive NMDARs.*

A) Example average EPSCs recorded at negative and positive potentials. Magenta are double exponential fits to the EPSC decay.

B) Decay time constants for n=5 cells recorded at positive and negative voltages.

C) R-CPP powerfully accelerates the decay τ of descending EPSCs recorded at positive potentials. The remaining fast EPSC is blocked by NBQX, indicating it is mediated by AMPA/kainate receptors.

D) Summary data for the effect of R-CPP on EPSC decay τ in n = 7 cells.

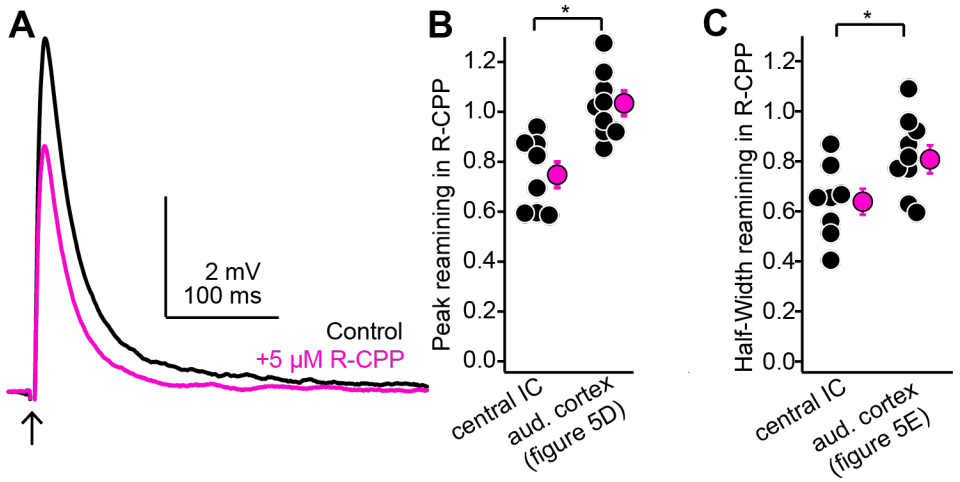

Figure 6 – Figure Supplement 1. *R-CPP has a greater effect on intra-collicular EPSPs evoked with single shock compared to descending EPSPs evoked with single light flashes.*

A) Example average traces of EPSPs recorded in a shell IC neuron following a single shock to the central IC before (black) and after (magenta) bath application of 5 μM R-CPP.

B) Fraction of peak EPSP amplitude remaining following 5 μM R-CPP for single evoked EPSPs at intra-collicular or auditory cortical synapses onto shell IC neurons. Asterisk denotes statistical significance (see main text).

C) Same as panel B, but for the fraction of EPSP half-width remaining in R-CPP. Values for auditory cortical EPSPs in panels B and C are from the same experiments as shown in Figures 5C-E.

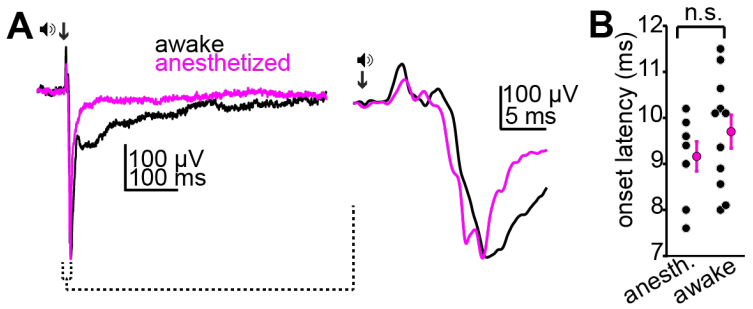

Figure 7 – Figure Supplement 1: *Urethane anesthesia does not impact the onset of acoustic activity in the superficial IC.*

A) Example average LFPs from the superficial IC of awake (black) or anesthetized (magenta) mice following a sound click (arrow). Inset: Rising phase and peak of the two waveforms at a faster time base. Of note is the similar onset latency of the LFP signal across the two example traces.

B) Summary data showing similar onset latencies of click-evoked LFPs in N=8 anesthetized and N=11 awake mice.

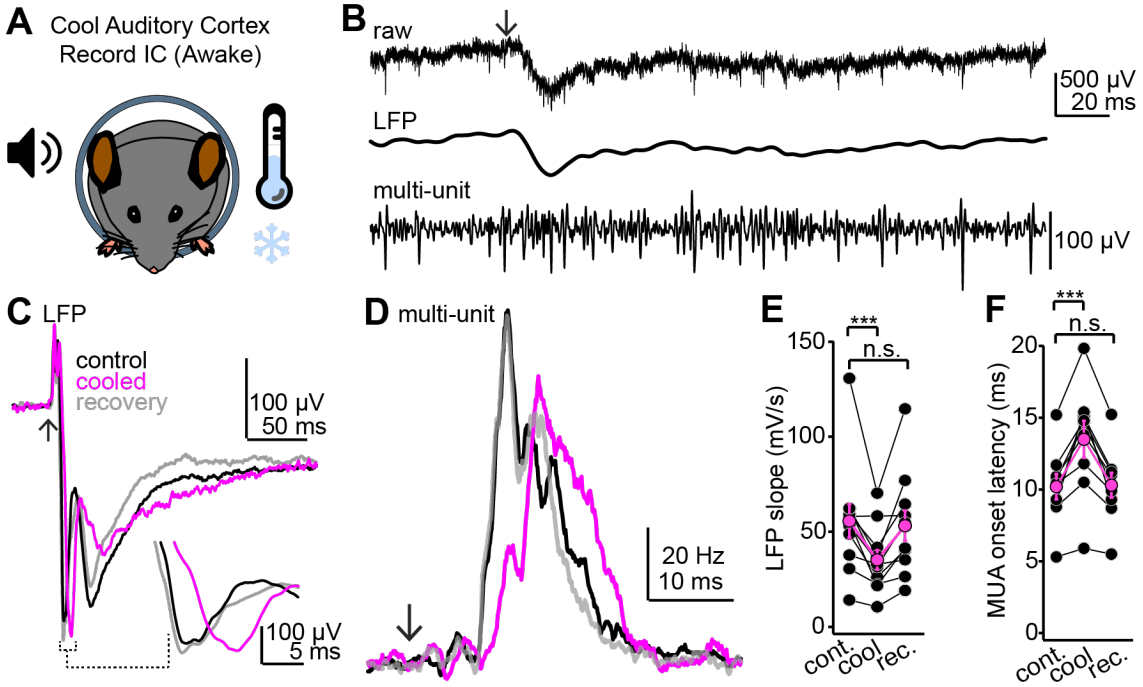

Figure 7 – Figure Supplement 2: *Cooling the auditory cortex impacts sound-evoked responses in the superficial IC of awake mice.*

A) Cartoon of experiment. Extracellular recordings are obtained from the IC of awake mice; peltier devices (not shown) are positioned bilaterally onto the auditory cortices.

B) Single trial from an example experiment. Top trace shows the raw extracellular waveform obtained following a click sound (arrow). Middle and lower traces are the LFP and multi-unit spike activity obtained following digital filtering (see Methods).

C) Example average LFP traces before (black), during (magenta), and after (gray) auditory cortical cooling. Inset shows the rising phase of the LFP at a faster time base to highlight the decrease in slope during cooling. Data are from a different experiment as the one shown in B. Arrow denotes click onset.

D) Multi-unit PSTHs following click onset (arrow) before, during and after auditory cortical cooling. Data are from the same recording as that of panel C. Of note is that the increase in multi-unit spiking is reversibly delayed by cooling, suggesting that auditory cortex indeed influences first spike latencies in the IC.

E,F) Group data quantifying the effect of auditory cortical cooling on LFP slope (E) and onset of multi-unit spiking (F). Asterisks denote statistical significance (Dunnett's test following one-way repeated measures ANOVA, p=0.006 and 0.0016 for E and F, respectively).